HHS Public Access

Author manuscript

Science. Author manuscript; available in PMC 2023 July 11.

Published in final edited form as:

Science. 2022 November 11; 378(6620): eabn5647. doi:10.1126/science.abn5647.

Enhanced T Cell Effector Activity by Targeting Mediator Kinase Module

Katherine A. Freitas[1,2,15], **Julia A. Belk**[9,15], **Elena Sotillo**[2], **Patrick J. Quinn**[2], **Maria C. Ramello**[2], **Meena Malipatlolla**[2], **Bence Daniel**[6,10], **Katalin Sandor**[10], **Dorota Klysz**[2], **Jeremy Bjelajac**[2,13], **Peng Xu**[2], **Kylie A. Burdsall**[2], **Victor Tieu**[3], **Vandon T. Duong**[3], **Micah G. Donovan**[11], **Evan W. Weber**[2,4,14], **Howard Y. Chang**[4,6,7], **Robbie G. Majzner**[2,5], **Joaquin M. Espinosa**[11,12], **Ansuman T. Satpathy**[2,4,10,16], **Crystal L. Mackall**[2,4,5,8,16,*]

[1]Immunology Graduate Program, Stanford University School of Medicine, Stanford, CA, USA

[2]Center for Cancer Cell Therapy, Stanford Cancer Institute, Stanford University School of Medicine, Stanford, CA, USA

[3]Department of Bioengineering, Stanford University School of Medicine, Stanford, CA, USA

[4]Parker Institute for Cancer Immunotherapy, San Francisco, CA, USA

[5]Division of Pediatric Hematology/Oncology/Stem Cell Transplant and Regenerative Medicine, Department of Pediatrics, Stanford University School of Medicine, Stanford, CA, USA

[6]Center for Personal Dynamic Regulomes, Stanford University, Stanford, CA, USA

[7]Howard Hughes Medical Institute, Stanford University, Stanford, CA, USA

[8]Division of BMT and Cell Therapy, Department of Medicine, Stanford University School of Medicine, Stanford, CA, USA

[9]Department of Computer Science, Stanford University, Stanford, CA, USA

[10]Department of Pathology, Stanford University School of Medicine, Stanford, CA, USA

[11]Department of Pharmacology, University of Colorado Anschutz Medical Campus, Aurora, Colorado, USA

[*]Correspondence should be addressed to cmackall@stanford.edu.

Author contributions: Conceptualization: KAF, CLM, ES, ATS, RGM, EWW. Methodology: KAF, JAB, BD, KS, DK, PX, EWW, RGM, MM, ATS. Investigation: KAF, JAB, BD, KS, DK, PX, MM, VTD, ES, KAB, MGD, MCR, JB, PJQ, KAB, MD. Visualization: KAF, JAB, VTD, VT. Writing – original draft: KAF, ES, CLM. Writing – review & editing: KAF, ES, CLM, EWW, HYC, RGM, ATS, JAB, JME.

Competing interests: K.A.F., E.S., and C.L.M. are coinventors on patent application number PCT/US2021/058047 submitted by the Board of Trustees of the Leland Stanford Junior University that covers the use of T cells deficient in *MED12* or *CCNC* for cancer immunotherapy. C.L.M. holds multiple patents in the arena of CAR T cell therapeutics. C.L.M. is a cofounder and holds equity in Lyell Immunopharma, Syncopation Life Sciences and Link Cell Therapies, which are developing CAR-based therapies, and consults for Lyell, Syncopation, Link, NeoImmune Tech, Apricity, Nektar, Immatics, Mammoth and Ensoma. A.T.S. is a cofounder of Immunai and Cartography Bio. A.T.S. receives research funding from Allogene Therapeutics and Merck Research Laboratories. H.Y.C. is an inventor on patents for the use of ATAC-seq, H.Y.C. is a co-founder of Accent Therapeutics, Boundless Bio, and an advisor for 10x Genomics, Arsenal Biosciences, Cartography Bio and Spring Discovery. E.W.W. consults for and holds equity in Lyell Immunopharma and VISTAN Health and consults for Umoja Biopharma. E.S. consults for and holds equity in Lyell Immunopharma and consults for Lepton Pharmaceuticals and Galaria. R.G.M. is a co-founder of and holds equity in Syncopation Life Sciences and Link Cell Therapies. RGM has served as a consultant for Lyell Immunopharma, Zai Labs, NKarta, Arovella Pharmaceuticals, Innervate Radiopharmaceuticals, GammaDelta Therapeutics, Immunai, and Aptorum Group. J.A.B. is a consultant to Immunai.

[12]Linda Crnic Institute for Down Syndrome, University of Colorado Anschutz Medical Campus, Aurora, Colorado, USA

[13]Institute for Stem Cell Biology & Regenerative Medicine, Stanford University School of Medicine, Stanford, CA, USA

[14]Present address: Department of Pediatrics, University of Pennsylvania, Philadelphia, PA 19104, USA

[15]These authors contributed equally: KAF and JAB

[16]These authors contributed equally: ATS and CLM

Abstract

T cells are the major arm of the immune system responsible for controlling and regressing cancers. To identify genes limiting T cell function, we conducted genome-wide CRISPR knock-out screens in human CAR-T cells. Top hits were *MED12* and *CCNC*, components of the Mediator cyclin-dependent kinase (CDK) module. Targeted *MED12* deletion enhanced anti-tumor activity and sustained the effector phenotype in CAR- and TCR-engineered T cells, and inhibition of CDK8/19 kinase activity increased expansion of non-engineered T cells. *MED12* deficient T cells manifested increased core Meditator chromatin occupancy at transcriptionally active enhancers, most pronounced for STAT and AP1 transcription factors, and increased *IL2RA* expression and IL-2 sensitivity. These results implicate Mediator in T cell effector programming and identify the CDK module as a target for enhancing potency of anti-tumor T cell responses.

One Sentence Summary:

The Mediator kinase module is a primary regulator of T cell effector function, and genetic or chemical inhibition of this module enhances T cell potency.

Introduction

T cell based immunotherapies, including immune checkpoint inhibitors and adoptive cell therapies, have demonstrated impressive antitumor effects in many cancers(1–8), but durable responses are not achieved in most patients. A central barrier to progress is limited T cell potency, resulting from a myriad of factors including T cell exhaustion, senescence, anergy and local and systemic immunosuppression(9–12). Advances in understanding the biology of T cell exhaustion are providing novel approaches to prevent this phenomena, including overexpression of c-JUN(13), deletion of NR4A(14), and transient induction of T cell rest(15, 16). However, it remains unclear whether exhaustion resistance will be sufficient to overcome the multitude of immunosuppressive factors within the tumor microenvironment.

Gene editing technologies are providing unparalleled opportunities to engineer more potent human T cells. *Ex vivo* CRISPR has been used safely to deliver gene-edited tumor-specific T cells to humans with cancer(17), and the CRISPR platform has been optimized to conduct forward genetic screens in primary human T cells to identify novel targets to augment T cell function. These approaches have identified genes that regulate PD-1 expression, T cell proliferation and persistence, and resistance to adenosine-mediated

immunosuppression(18–20), but work is ongoing to define genes for which editing will most potently augment anti-tumor responses in humans. We utilized CRISPR screening to identify genes that regulate effector function in primary human T cells expressing chimeric antigen receptors (CARs) and discovered that *MED12* and *CCNC*, genes encoding proteins in the CDK module of the Mediator complex, negatively regulate T cell effector activity. Mediator, an evolutionarily conserved multi-subunit protein complex that acts as a bridge between enhancer-bound transcription factors and the general transcription machinery, is required for gene transcription and plays a central role in establishing cellular identity by coordinating transcriptional networks(21–23). Across multiple CAR-T cell models with different costimulatory domains, and in T cells expressing a recombinant T cell receptor, we discovered that genetic disruption of the CDK module of Mediator induced transcriptional and epigenetic changes that resulted in enhanced effector function, metabolic fitness, and increased anti-tumor activity. Small molecule mediated inhibition of CDK8/19 in non-engineered T cells phenocopied several of these enhancements. These results implicate the Mediator CDK module as a therapeutic target for augmenting T cell fitness and identify a previously unknown role for *MED12* in regulating human T cell function.

Results

Genome-wide screen identifies the Mediator CDK module as a regulator of CAR-T cell expansion and cytokine production.

To identify genes which restrain CAR-T cell function, we performed two genome-wide CRISPR deletion screens to identify negative regulators of T cell expansion and cytokine production in primary T cells from two donors transduced with HA-28ζ, a high affinity GD2-targeting CAR that induces functional, transcriptomic and epigenetic hallmarks of T cell exhaustion(13, 16). Using a previously published sgRNA library(24), editing was achieved by adapting the SLICE platform (single guide RNA (sgRNA) lentiviral infection with Cas9 protein electroporation)(18) to incorporate CAR transduction (Fig. 1A and fig. S1A). We detected 98% of the sgRNA library in transduced CAR-T cells, with 19,885 genes targeted by at least 4 sgRNAs (Fig. S1B and fig. S1C). Successful editing was confirmed by drop out of sgRNAs targeting a “gold standard” set of essential genes but not control guides after 23 days in culture (fig. S1D, Table S1–S2).

For the expansion screen, we cultured the transduced cells *in vitro* for 15 days, then co-cultured with $GD2^+$ tumor cells until day 23 and compared sgRNA abundance between day 0 and day 23 (fig. S1E). Using the MAGeCK algorithm(25) both donors showed enrichment of sgRNAs targeting genes known to inhibit T cell survival, such as *FAS* and *CASP3*(26) (Fig. 1B), while sgRNAs targeting genes known to promote T cell proliferation, such as *IL2RG*, *MYC* and *ZAP70*, were depleted. The top hits in the expansion screen were *CCNC* and *MED12*, members of the CDK module of Mediator, with 7 out of 7 guides targeting *CCNC* and 8 out of 8 guides targeting *MED12* positively enriched (figs. S2A–C). The expansion screen also showed depletion of sgRNAs targeting *BATF* and *JUNB*, suggesting a survival role for AP-1 family members in the setting of chronic stimulation.

In the cytokine production screen, we cultured HA-28ζ CAR-T cell knock-out libraries *in vitro* for 15 days, added $GD2^+$ tumor cells to the culture for 6 hours, used FACS to sort cells

and compared sgRNA abundance in CAR-T cells expressing IL-2 and TNFα protein against the total population (fig. S1E). *MED12* was enriched in the cytokine screen, with 6 out of 7 guides demonstrating enrichment, while several genes, including 9 out of 9 guides targeting *ZAP70* were depleted, consistent with the known role for *ZAP70* in CAR signaling(27) (Fig. 1C and figs. S2B–C). Six of 9 guides targeting *TNF* and 5 out of 8 guides targeting *IL2* were also significantly depleted, demonstrating an expected loss of cytokine-negative cells in the sorted population (fig. S2B).

Mediator consists of a 26 subunit core organized into head, middle, backbone, and tail domains, and a 4 subunit dissociable kinase module(28, 29) (Fig. 1D). *CCNC* and *MED12* are both centrally located in the kinase module(30), suggesting that loss of either gene disrupts a common function. Consistent with this, sgRNAs targeting all members of the kinase module were positively enriched in the expansion screen except for *MED12L*, which is not expressed in T cells (Fig. 1E and fig. S2D). In contrast, sgRNAs targeting subunits of the head, backbone, and middle domains of core Mediator were associated with poor expansion (Fig. 1E). Together, these data demonstrated a requirement for the core Mediator complex in T cell survival and a regulatory role for the Mediator kinase module in T cell expansion and cytokine production.

MED12 deficient and CCNC deficient CAR-T cells demonstrate increased in vitro and in vivo expansion independent of co-stimulation domain or tonic CAR signaling.

To validate the expansion screen findings, sgRNAs targeting *CCNC*, *MED12*, or *AAVS1* as a control, were delivered as ribonucleoprotein 3 days after T cell activation followed by retroviral transduction of the HA-28ζ CAR (fig. S3A). *CCNC* and *MED12* deletion were confirmed by immunoblotting and Sanger sequencing using Inference of CRISPR Edits (ICE)(31) (figs. S3B–C). Because CAR transduction efficiency, as well as the ratio of $CD4^+$ to $CD8^+$ cells, could impact CAR-T cell function, we confirmed loss of *MED12* or *CCNC* did not change CAR expression or the ratio of $CD4^+$ to $CD8^+$ cells, nor did it impact retroviral integration of GFP (figs. S3D–H). *MED12* and *CCNC* deficient HA-28ζ CAR-T cells showed greater expansion compared to control cells over 23 days in culture (Fig. 2A). We previously reported that HA-28ζ CAR-T cells develop hallmark features of exhaustion due to tonic signaling(13, 16, 32). To determine whether MED12 and/or CCNC would limit functionality of CAR-T cells that do not develop exhaustion *in vitro*, we deleted *MED12* and *CCNC* in T cells expressing the CD19–28ζ CAR (13, 16, 32). *CCNC* and *MED12* deficient CD19–28ζ CAR-T cells demonstrated increased expansion compared to control cells over 23 days in culture and following serial stimulation with tumor cells (Fig. 2A and fig. S4A). Furthermore, adoptively transferred *MED12* and *CCNC* deficient HA-28ζ and CD19–28ζ CAR-T cells showed increased *in vivo* expansion in tumor-bearing NSG mice compared with control CAR-T cells (fig. S4B). We also observed enhanced expansion of *MED12* and *CCNC* deficient HER2–4-1BBζ CAR-T cells (fig. S4B), confirming that the findings are not restricted to CAR-T cells incorporating a CD28 costimulatory domain. Together, these results demonstrate that *MED12* and *CCNC* deficient human CAR-T cells manifest enhanced antigen-driven expansion regardless of whether the CAR incorporates a CD28 or 4–1BB co-stimulatory domain or if the CAR-T cells manifest hallmark features of exhaustion.

To determine if these effects are dependent on catalytic activity of the CDK module, we cultured healthy human T cells following anti-CD3/CD28 activation with compounds that are dual inhibitors of CDK8 and CDK19 and observed significant increases in T cell expansion (Fig. 2B). Additionally, overexpression of *MED12* suppressed T cell proliferation, confirming the CDK module restrains T cell expansion (figs. S4C–D). *MED12* and *CCNC* behave as tumor suppressors in some settings(33, 34), however when we removed IL-2 from the culture medium, we observed a complete loss of viable cells within 3 weeks (fig. S4E), indicating that expansion is not associated with transformation as the cells remain IL-2 dependent. Together, these results demonstrate that the CDK module is a potent modulator of human T cell expansion.

CCNC deficient and MED12 deficient CAR-T cells produce higher levels of inflammatory cytokines following antigen stimulation.

Next, we sought to confirm the effects of *MED12* and *CCNC* deletion on antigen-induced cytokine production using bulk assays and by assessing single cell production of IL-2 and TNFα by flow cytometry. Bulk cultures of antigen stimulated *MED12* and *CCNC* deficient HA-28ζ, CD19–28ζ and HER2–4-1BBζ CAR-T cells produced higher levels of cytokines and showed increased frequencies of IL-2 and TNFα expressing cells (Fig. 2C and figs. S5A–B). Additionally, we found elevated *IL2*, *IFNG*, and *TNF* mRNA levels in *MED12* deficient cells compared with control cells, indicating these changes are transcriptionally mediated (fig. S5C). To assess the impact of Mediator kinase module disruption more broadly on antigen-induced cytokine secretion, we performed bead-based multiplex immunoassay profiling of 38 cytokines in supernatants collected from CD19–28ζ CAR-T stimulated with $CD19^+$ Nalm6 leukemia cells for 24 hours. Hierarchical clustering showed that the cytokine profile of *MED12* and *CCNC* deficient CD19–28ζ CAR-T cells was distinct from controls (Fig. 2D), with increased proinflammatory cytokines including IFNγ, TNFα, IL-17, IL-6, increased inflammatory chemokines CXCL10 and CCL3, and increased common gamma chain family cytokines IL-2 and IL-9, which promote T cell survival and differentiation (fig. S5D). Together, these results demonstrate that *MED12* and *CCNC* constrain antigen induced T cell expansion and inflammatory cytokine production and raise the prospect that *MED12* or *CCNC* deficient T cells may demonstrate enhanced anti-tumor immune responses.

CCNC deficient and MED12 deficient CAR-T cells demonstrate increased metabolic fitness and anti-tumor activity.

To assess whether *MED12* or *CCNC* deficient T cells manifest metabolic features of enhanced effector functionality(35), we measured glycolytic and oxygen consumption rates. We observed increased basal and maximal oxygen consumption in *MED12* and *CCNC* deficient cells, despite no change in mitochondrial mass, and increased basal and maximal rates of glycolysis (Figs. 2E–F and figs. S6A–B). Stimulation of CD19–28ζ CAR-T cells via the CAR resulted in higher levels of pS6 in *MED12* deficient cells, demonstrating enhanced antigen-dependent activation of the MTORC1 pathway which may contribute to the increased metabolic activity observed (figs. S6C–D). The simultaneous increases in rates of oxidative phosphorylation and glycolysis observed in *MED12* deficient cells is similar to

the metabolic state described in early activated T cells, which have not yet differentiated into short lived effector cells or memory cells(36).

CCNC and *MED12* deficient CAR-T cells demonstrated enhanced anti-tumor function *in vivo*, in a model wherein NSG mice were inoculated with Nalm6 or Nalm6-GD2 leukemic cells and treated 3 days later with gene-edited CD19–28ζ or HA-28ζ CAR-T cells respectively (Figs. 2G–H and figs. S6E–F). Similarly, we observed enhanced tumor control and prolonged survival in mice engrafted with 143B osteosarcoma cells and treated with *MED12* and *CCNC* deficient CAR-T cells expressing the HER2–4-1BBζ receptor (Fig. 2I and fig. S6G). Collectively, these results demonstrate that *MED12* and *CCNC* deficient T cells manifest enhanced hallmark features of effector cells, spanning antigen induced expansion, cytokine production, metabolic fitness and killing capacity.

MED12 deficient T cells demonstrated sustained effector function under chronic stimulation.

To further investigate the impact of CDK module disruption on longer term T cell fitness and following repetitive antigen stimulation, we focused on *MED12* because this gene was a top hit in both CRISPR screens. MED12 deficient HA-28ζ CAR-T cells demonstrated increased expansion and cytotoxicity following repeated stimulation with Nalm6-GD2 tumor cells (Figs. 3A–B and figs. S7A–B). Similarly, *MED12* deficient HA-28ζ CAR-T cells cultured *in vitro* until day 54 continued to demonstrate enhanced T cell expansion and cytokine production (Figs. 3C–D). To further characterize the *MED12* deficient phenotype at late timepoints, we performed single cell proteomic analysis of 34 proteins using mass cytometry to measure lineage-defining transcription factors and cell surface markers associated with activation, exhaustion, and T cell differentiation (Table S3). Both control and MED12 deficient HA-28ζ CAR-T cells displayed an activated effector phenotype after 50 days in culture, with high expression of Ki67, CD69, Tbet, TOX, CD25, and CD122, and low expression of IL7R, CD45RA, CD27, CD28, CCR7, and TCF7 relative to non-activated T cells isolated from peripheral blood (figs. S7C–D). Relative to control HA-28ζ cells, loss of *MED12* strikingly reduced expression of CD39, a marker associated with terminal exhaustion and diminished stemness (Figs. 3E–F)(37, 38), while PD-1 and TIM3 were unchanged, and LAG3 was elevated (fig. S7E). Additionally, *MED12* deficient cells maintained an elevated $CD8^+$ to $CD4^+$ ratio during long-term culturing (fig. S7F).

To determine whether cells lacking *MED12* would manifest sustained anti-tumor activity *in vivo*, we engrafted mice with Nalm6-GD2 leukemia, treated with *MED12* deficient or control HA-28ζ CAR-T cells, and rechallenged with additional tumor cells 26 days after CAR-T cells were administered. *MED12* deficient CAR-T cells protected from rechallenge with $GD2^+$ but not $GD2^-$ tumor cells, demonstrating prolonged antigen-specific anti-tumor activity (Figs. 3G–I). Together, these results show that loss of MED12 results in long-term enhancement of T cell fitness, both in the setting of chronic stimulation due to the tonic signaling HA-28ζ CAR and following repeated encounters with tumor cells.

Loss of MED12 increases effector function in T cells utilizing a TCR for tumor recognition.

To determine if the effects observed in *MED12* deficient CAR-T cells were generalizable to T cells that utilize a TCR for target recognition, we deleted *MED12* and transduced cells with the alpha and beta chains of a TCR that recognizes New York esophageal squamous cell carcinoma (NY-ESO-1), a tumor antigen found in numerous human cancers including melanoma and synovial sarcoma(39). Compared to controls, *MED12* deficient NY-ESO-1 T cells demonstrated an increased proportion of cells bearing an effector memory phenotype ($CCR7^{+}CD45RO^{+}$), and a lower proportion bearing a stem cell memory phenotype (Fig. 4A–B and fig. S8A). *MED12* deficient NY-ESO-1 T cells showed reduced expression of CD45RA and IL7R, and elevated expression of Ki67, IL2RA, ICOS, and Tbet, consistent with an activated, proliferating, effector phenotype with diminished quiescence compared to control cells (Figs. 4C–E and figs. S8B–C).

Loss of *MED12* resulted in increased T cell expansion in culture and increased cytokine release upon co-culture with NY-ESO-1^{+} melanoma cells (Figs. 4F–G). To determine if loss of *MED12* increased anti-tumor activity *in vivo*, we engrafted mice with A375 melanoma and treated with control or *MED12* deficient NY-ESO-1 T cells. Complete tumor clearance was observed 28 days after treatment in 7 of 9 mice in the *MED12* deficient group, while 0 of 9 mice were tumor-free in the control group (Figs. 4H–I and fig. S8D). Single-cell transcriptomic profiling of tumor infiltrating NY-ESO-1 T cells showed that *MED12* deficient cells expressed higher levels of genes encoding cytotoxic molecules including perforin, granzyme B, and interferon gamma, and lower levels of natural killer cell receptors *KLRD1* and *KLRB1*, which have been associated with T cell dysfunction during chronic antigen exposure (Figs. 4J–K and fig. S8E)(40), and cell cycle analysis showed a higher fraction of *MED12* deficient TILs were in S phase, consistent with increased proliferation in tumors (fig. S8F).

To assess similarities between *MED12* deficient T cells and naturally occurring T cell populations found in tumors from human donors, we compared the scRNA-seq profiles of control and *MED12* deficient NY-ESO-1 T cells isolated from xenograft tumors to a set of 17 previously described T cell gene expression signatures (41). *MED12* deficient T cells were enriched for the interferon stimulation gene signature and depleted in the NK-like T cell signature, consistent with our previous observations. We also found modest enrichment of the $GZMK^{+}$ early T effector memory signature, which supports the model that loss of *MED12* sustains a transitory effector memory phenotype that precedes terminal effector differentiation (Fig. S8G–H). Together, the data demonstrate phenotypic differences and functional enhancements observed in *MED12* deficient CAR-T cells are generalizable to T cells expressing a recombinant TCR and indicate that disruption of the CDK module could have broad utility in T cell directed immunotherapies.

MED12 deficient CAR-T cells have an effector-like phenotype and display an activated transcriptional program.

MED12 deficient CAR-T cells displayed effector phenotypes based upon an absence of CCR7; however, *MED12* deficient CAR-T cells expressed high levels of CD45RO, while control cells were largely negative for this marker at this timepoint(42–44)(Figs.

5A–B). Both *MED12* deficient and control CD19–28ζ CAR-T cells expressed high levels of Blimp-1 and low levels of Eomes and CD28, consistent with an effector phenotype(45); however, unbiased clustering demonstrated significant distinctions between *MED12* deficient and control phenotypes (Fig. 5C and fig. S9A). *MED12* deficient cells expressed higher levels of T-bet, ICOS, TOX, and CD45RO, and lower levels of CD45RA and IL7R, a phenotype previously associated with short lived effector cells (SLECs) that have not undergone terminal differentiation(46) (Fig. 5D and figs. S9B–C). Paradoxically, *MED12* deficient cells also expressed high levels of CD62L, which is usually associated with stem cell and central memory subsets and not typically expressed by SLECs. *MED12* deficient CD19–28ζ CAR-T cells also expressed high levels of LAG-3, while other exhaustion markers PD-1, TIM3, TIGIT, and CD39 were lowly expressed and unchanged from control cells (Fig. 5D and fig. S9C). Together, these results demonstrate that *MED12* deficient CAR-T cells manifest expansion of a unique $CCR7^{-}IL7R^{-}Tbet^{+}ICOS^{+}CD62L^{+}$ effector cell subset that displays enhanced cytokine production, effector cell potency, metabolic fitness, and antitumor activity.

To assess genome-wide transcriptional differences between *MED12* deficient and control cells, bulk RNA-seq was performed on day 15 CD19–28ζ CAR-T cells following a 3-hour stimulation via the CAR *in vitro*. *MED12* deficient cells were transcriptionally distinct from control cells with differential expression of 3501 genes between genotypes in at least one condition (Fig. 5E). Consistent with the functional and phenotypic data, *MED12* deficient cells demonstrated increased expression of numerous genes associated with effector cell differentiation, including AP-1 family transcription factors (*FOS, JUNB, BATF, BATF3*), *IFNG, TNF, CD38, IL2RA*, and *CD69.* They also expressed lower levels of genes associated with T cell stemness including *LEF1, TCF7, CD27, IL7R*, and decreased expression of genes associated with T cell quiescence including *KLF2* and *FOXO1.* Consistent with *MED12* deficient cells manifesting enhanced cytokine secretion and metabolic fitness, gene set enrichment analysis of differentially expressed genes revealed enrichment of metabolic and cytokine-related gene sets (Figs. 5F–G). Transcriptional changes induced by loss of MED12 were largely shared between $CD4^{+}$ and $CD8^{+}$ T cell subsets (figs. S9D–F). Together, these results indicate loss of MED12 promotes an activated effector memory phenotype with enhanced metabolic fitness and cytokine secretion capacity.

Loss of MED12 increases core Mediator chromatin occupancy at transcriptionally active enhancers.

The Mediator complex lacks a DNA binding domain, but interacts with chromatin through protein-protein interactions with DNA-bound transcription factors and RNA polymerase II (RNAPII)(47). To identify the genomic locations of chromatin-Mediator interactions, we performed ChIP-seq using antibodies against MED12 and MED1 to profile chromatin binding of the kinase module and core Mediator, respectively, in the presence or absence of MED12. Comparison of MED1- and MED12-bound genomic regions in control CD19–28ζ CAR-T cells showed MED1/MED12 co-localization in 86.1% of sites, while MED1 was found exclusively at 13.1% of sites and MED12 was found exclusively at only 0.7% of sites (Fig. 6A). These results demonstrate that, in human T cells, the CDK module rarely contacts chromatin in the absence of core Mediator and the CDK module is present at the majority of

sites occupied by core Mediator. Given the degree of co-localization observed, we predicted that *MED12* deletion could have widespread effects on transcription and function of the core Mediator.

To assess the effect of *MED12* deletion on core Mediator chromatin occupancy, we compared genomic regions bound by MED1 in control and *MED12* deficient CAR-T cells. PCA showed global differences in MED1 occupancy between genotypes including 842 sites with increased MED1 occupancy and 270 sites with decreased MED1 occupancy (Fig. 6B and fig. S10A), demonstrating a general pattern of increased MED1 binding in the absence of MED12. Consistent with a model wherein the CDK module limits access of core Mediator to chromatin, *MED12* deficient cells showed approximately a two-fold increase in MED1 ChIP-seq signal intensity at sites where increased MED1 binding was observed (Fig. 6C). Increased MED1 chromatin binding was confirmed by immunoblotting studies, which demonstrated that compared with control cells, *MED12* deficient cells had more abundant MED1 in the chromatin-bound fraction and in total cell lysates, but *MED1* transcript was not differentially expressed, indicating this effect was post-transcriptionally regulated (Fig. 6D–E and figs. S10B–D).

To determine if sites with increased MED1 chromatin occupancy following *MED12* deletion represent transcriptionally active regions, we performed ChIP-seq with antibodies targeting H3K27ac and RNAPII pS2 (the elongating form of RNAPII). Consistent with a model wherein *MED12* deletion modulates transcription at MED1 bound sites, we observed that sites with changes in MED1 ChIP-seq signal were highly concordant with sites demonstrating differences in H3K27ac ChIP-seq, RNAPII ChIP-seq, and ATAC-seq, indicating changed transcriptional activity (Fig. 6F and figs. S10E–F). Pathway analysis of the genes located near sites with increased MED1 occupancy showed enrichment of genes related to T cell differentiation, cytokine receptor signaling, and immune response genes (Fig. 6G, Table S5) and included many genes with significantly increased transcript levels, including *IFNG*, *IL17F*, *IL2RA*, and *TOX* (Fig. 6H and fig. S10G). Together, the data are consistent with a model wherein loss of *MED12* increases MED1 chromatin occupancy at select sites in human T cells responsible for regulating T cell differentiation, leading to transcriptional reprogramming of CAR-T cells and enhanced potency.

Loss of MED12 increases STAT5 activity in CD19–28ζ CAR-T cells

To define the most differentially regulated transcriptional programs in *MED12* deficient cells, we used HOMER motif enrichment analysis to identify differentially accessible transcription factor binding motifs in *MED12* deficient vs. control cells. The top enriched motifs were STAT5 and STAT1, transcription factors that drive cytokine mediated gene expression (Figs. 7A–B and figs. S11A–C). AP-1 family motifs including JunB, BATF, and FOS were also significantly enriched, as well as motifs from Interferon Response Family (IRF) members such as IRF8 and IRF4. Motif enrichment analysis on sites with increased MED1 occupancy in MED12 deficient cells also showed enrichment of STAT and AP-1 motifs (Fig. 7C), confirming that core Mediator is recruited to these sites. Some motifs demonstrated decreased accessibility in *MED12* deficient cells, including FLI1 and FOXO1, which are implicated in maintaining T cell quiescence (48, 49) (fig. S11D), providing

evidence that *MED12* deficiency also diminishes transcription of some genes. ATAC-seq profiling of sorted $CD4^+$ and $CD8^+$ CD19–28ζ CAR-T cells showed chromatin accessibility changes in *MED12* deficient cells were largely shared between subsets and indicated increased AP-1 and STAT family transcription factor signatures in both $CD4^+$ and $CD8^+$ T cells (fig. S12A–D).

To assess the functional significance of these findings, we compared STAT5 phosphorylation in *MED12* deficient vs. control cells during *in vitro* culture with IL-2 and observed that *MED12* deficient cells manifest significantly higher levels of phosphorylated STAT5 (Fig. 7D). STAT5 activation was dependent on IL-2, since removal of IL-2 for 24 hours reversed the effect, whereas brief re-exposure of *MED12* deficient CAR-T cells to IL-2 led to higher maximum levels of phosphorylated STAT5 compared to control cells (figs. S13A–B). *MED12* deficient CAR-T cells also manifested increased expression of the high-affinity IL-2 receptor, *IL2RA*, a downstream target of STAT5 mediated transcription, while expression of *IL2RG* was unchanged (Fig. 7E, fig. S13C) (50). Furthermore, activated heathy, non-transduced T cells also showed elevated *IL2RA* expression in the absence of *MED12*, indicating this effect was not dependent on CAR signaling (Fig. 7F), and T cells cultured with CDK8/19 inhibitors also showed elevated expression of *IL2RA*, demonstrating that inhibition of CDK8/19 kinase activity is sufficient to elicit increased sensitivity to IL-2 in human T cells (Fig. 7G).

We observed increased MED1 occupancy at the *IL2RA* locus in *MED12* deficient cells (Fig. 6H), and comparing sites with increased chromatin accessibility in *MED12* deficient cells to previously published STAT5 ChIP-seq data from $CD4^+$ T cells(51), we found extensive co-localization of MED1 and STAT5 (Figs. 7H–I). Together these results are consistent with a model wherein enhanced MED1 occupancy increases *IL2RA* expression in *MED12* deficient T cells, thereby initiating a feed-forward loop in which heightened sensitivity to IL-2 promotes STAT5 activation and prolonged upregulation of *IL2RA*. Together, these results demonstrate that *MED12* deletion regulates T cell effector differentiation and function by transcriptional reprogramming through modulation of MED1 chromatin occupancy. These effects are associated with enhanced activity of multiple transcription factors that control T cell fate during effector differentiation, including STAT5, as well as others such as AP-1, IRF, and other STATs (52–54).

Discussion

Immune checkpoint inhibitors and adoptive T cell therapies induce profound anti-tumor effects in some patients for whom all other therapies have failed, but most patients treated with cancer immunotherapies do not experience long-term benefits(1–5). Enhancing the efficacy of cancer immunotherapies requires new approaches to augment the potency of tumor-specific T cell responses. In the context of adoptive cell therapy, significant efforts have focused on enhancing stem-like pools of memory T cells and thereby increasing the supply of effector cells(55–57) and on preventing or reversing T cell exhaustion to enhance T cell function(13, 14, 16). Here, we used systematic, unbiased genome-wide CRISPR-Cas9 screens to identify targets capable of enhancing CAR-T cell effector function. Our results converged on *MED12* and *CCNC*, core components of the Mediator kinase module, which

have not previously been implicated in regulating T cell potency. Our screen also confirmed an expected requisite role for core Mediator in human T cell function.

To explain these findings, we demonstrated that the CDK module and core Mediator are largely co-localized in wildtype CAR-T cells, consistent with the known role for the CDK module in modulating the interaction between core Mediator and RNAPII(58, 59), and leading to the hypothesis that loss of *MED12* or *CCNC* in T cells reduces steric hindrance between core Mediator and RNAPII, and thereby increases transcription and modulates T cell function. Consistent with this model, deletion of *MED12* shared some phenotypic similarities with deletion of *CCNC*, although more profound effects were observed following *MED12* deletion, potentially due to the structural relationships that predict full ablation of the Mediator kinase module in the absence of *MED12*, and partial ablation upon *CCNC* deletion(30, 58, 60, 61). Our data demonstrate selective changes in the chromatin landscape and enhancement of MED1 binding to chromatin in *MED12* deficient T cells with the most profound seen in regulatory regions associated with transcription factors that regulate T cell differentiation. This selective but widespread pattern of modulation may explain why the Mediator kinase module was the top hit in our CRISPR screens, rather than any single transcription factor.

MED12 deletion selectively enhanced expression of numerous transcription factors involved in T cell effector differentiation, including TOX, T-bet, and BATF3, and orchestrated coordinated changes in chromatin accessibility and increased MED1 occupancy at motifs for several transcription factor families involved in T cell differentiation including STAT5, cJUN, BATF, and IRF8. We hypothesize that the effects of *MED12* and *CCNC* deletion are highly context dependent, since we observed increased glycolytic rates in *MED12* and *CCNC* deficient effector T cells, consistent with enhanced effector activity, whereas previous studies in cancer have demonstrated diminished glycolytic activity in several cancers following small molecule mediated inhibition of CDK8(62). The selectivity of the effects is not fully understood, but may be explained in part by the newly reported finding that enhancers have varying degrees of dependence on Mediator for transcriptional activation, determined by the presence of sequence-specific transcription factors and other chromatin characteristics(63).

Functional studies revealed elevated STAT5 activity in *MED12* deficient T cells, manifested as increased *IL2RA* expression and increased sensitivity of T cells to IL-2. We also observed significant alterations in effector T cell differentiation, with *MED12* deficient $CD4^+$ and $CD8^+$ cells demonstrating an early activated phenotype, comprising elevated expression of ICOS, Tbet, and CD25, along with simultaneous increases in glycolysis and oxidative phosphorylation(36). Paradoxically however, *MED12* deficient cells showed elevated CD62L and CD28, molecules not typically expressed on effector cells. This raises the possibility that *MED12* loss induces a *synthetic effector* state not represented by T cell phenotypes found in nature.

Current models hold that upon antigen encounter, naïve T cells differentiate into $CCR7^-IL7R^-Tbet^+CD62L^-$ short-lived effector cells (SLECs), with most effectors progressing toward a state of terminal differentiation associated with diminished activity,

while a fraction express CCR7 and IL7R and differentiate into long-lived memory cells(44, 46, 65, 66). The functionally enhanced *MED12* deficient effector CAR-T cells observed here displayed a unique $CCR7^{-}IL7R^{-}ICOS^{+}Tbet^{+}CD62L^{+}$ phenotype, with diminished expression of CD45RA (42). Of interest, $CD4^{+}ICOS^{+}Tbet^{+}LAG3^{+}$ cells similar to those described here have been implicated in mediating tumor regression in patients treated with anti-CTLA4 therapy(64). While *MED12* deficient cells showed increases in LAG3 and TOX, which have been associated with T cell exhaustion, we observed downregulation of CD39 and augmentation of numerous functional attributes spanning improved proliferation, cytokine secretion, and ultimately, sustained improvements in functionality even at late timepoints, improved tumor control *in vivo,* and long-term protection from antigen rechallenge. Together these data are not consistent with exacerbation of T cell exhaustion in *MED12* deficient T cells.

In summary, this work identifies the Mediator CDK module as a critical negative regulator of T cell effector differentiation and function. Deletion of either *MED12* or *CCNC* induces broad functional enhancements in effector T cells, including increased expansion, cytokine secretion, metabolic fitness, and sustained effector function during chronic stimulation, all properties that would be predicted to enhance antitumor effects. Pharmacological inhibition of Mediator kinase activity phenocopied genetic ablation of *MED12* in regards to increased expansion and elevated expression of *IL2RA*, raising the possibility of synergistic antitumor effects of such agents in the context of immunotherapy since hyperactive CDK8/19 kinase activity activates oncogenes in some cancer types(67). The work further implicates interactions between the CDK module and core mediator as a major axis of regulation of T cell differentiation. Technologies to inactivate genes in the context of *ex vivo* cell manufacturing and even *in vivo* gene editing(68), using a variety of approaches including CRISPR/Cas9, Zinc finger nucleases, TALENs, or base editing, are increasingly available for emerging applications in human medicine(69), highlighting the potential for clinical translation of these findings.

Materials and Methods

T cell isolation

Whole blood buffy coats were obtained from the Stanford Blood Center from healthy volunteers under 41 years. T cells were isolated using the RosetteSep Human T Cell Enrichment Cocktail (Stemcell Technologies). T cells were stored in CryoStor cell cryopreservation media CS10 (Sigma Aldrich*)* in liquid nitrogen.

CRISPR screen

T Cell activation and culturing—200 million T cells from each of two donors were thawed on day 0 and activated with CD3/CD28 Dynabeads (Invitrogen) at a ratio of three beads per T cell. Cells were cultured in AIM-V medium (Gibco) supplemented with 5% FBS, 10 mM HEPES, 1X penicillin-streptomycin-glutamine supplement (Gibco), and 10 ng/mL recombinant IL-2, (21.8 IU/mL) (Peprotech). Cells were maintained at a density between 0.5 and 2 million per mL in T175 flasks.

Lentiviral transduction—The complete Bassik Human CRISPR Knockout Library was obtained from Addgene and amplified with Endura ElectroCompetent Cells (Lucigen). LentiX cells (Takara) were plated on 150 mm plates coated with poly-D-lysine (Corning) and transfected with 18 μg REV, 18 μg GAG/POL, 7 μg VSVg, 15 μg library vector, 3.38 mL Opti-MEM (Gibco) and 135 μL Lipofectamine 2000 (Invitrogen) per plate. Media was changed 24 hours after transfection and supernatant was harvested 48 hours after transfection. Lentiviral supernatant was concentrated with Lenti-X Concentrator (Takara) and added to the T cell culture medium 2 days post activation. On day 3, cells were assessed for mCherry expression by flow cytometry to confirm the percentage of transduced cells was between 8 and 12%.

CAS9 electroporation—On day 3, 100 μl reactions were assembled with 10 million T cells, 30 μg Alt-R S.p. Cas9 Nuclease V3 (IDT), 90 μl P3 buffer (Lonza), and 7 μL Duplex Buffer (IDT). Cells were pulsed with protocol EO115 using the P3 Primary Cell 4D-Nucleofector Kit and *4D Nucleofector* System (Lonza). Cells were recovered immediately with warm media for 6 hours prior to transduction with CAR. The electroporation protocol was repeated on day 5.

Retroviral Transduction—Retroviral supernatant was produced as previously described(13). Briefly, 293GP cells were plated on poly-D-lysine (Corning) coated plates and transfected with RD114 envelope and HA-28ζ CAR encoding plasmids using Lipofectamine 2000 (Invitrogen). Media was changed 24 hours after transfection and supernatant was harvested 48 and 72 hours after transfection. On days 3 and 4, tissue culture plates were coated with RetroNectin (Takara), blocked with 2% BSA for 5 minutes, and incubated with retroviral supernatant for 2 hours at 32°C, 3200 rpm. T cells were added to virus coated plates at a density of 1×10^6 per mL. On day 5, CD28/CD3 Dynabeads (Invitrogen) were removed using magnetic separation. Cells were cultured with puromycin at 2.5 μg/mL from days 7 to 10 to eliminate cells which did not express a guide.

Expansion Screen—The CAR-T cells transduced with the sgRNA library were cultured in T175 flasks and were passaged every other day. On day 15, 100 million NALM6-GD2 cells were added to 100 million T cells and co-cultured to day 23. 50% of the culture volume was discarded at each passage. On day 23, duplicate samples of 30 million cells were collected for genomic DNA extraction. The plasmid DNA encoding the lentiviral sgRNA library was used to approximate the relative abundance of sgRNAs at the start of the experiment.

Cytokine Production Screen—On day 15, duplicate samples of 30 million cells from each of two donors were harvested from the total population for genomic DNA extraction. 100 million CAR-T cells were co-cultured for 6 hours with 100 million NALM6-GD2-GFP tumor cells with eBioscience Monensin Solution (Invitrogen) in 200 mL medium without IL-2. Intracellular cytokine staining was performed using the Cytofix/Cytoperm Kit (BD). Cells were stained with antibodies specific for CD4, CD8, TNF-α, and IL-2 (Table S4), and fixable viability dye eFluor506 (eBioscience). Cell sorting was performed at the Stanford Shared FACS Facility on a FACSAria II equipped with a 70μm nozzle. The top 10% of

TNFα$^+$ and IL-2$^+$ were sorted using individual gates for CD4$^+$ and CD8$^+$ cells. CD4$^+$ and CD8$^+$ cytokine high cells were pooled. A single sorted sample of approximately 5 million TNFα$^+$ IL-2$^+$ cells were collected from each donor for genomic DNA extraction.

Genomic DNA extraction and sequencing library preparation—Technical duplicates were performed for genomic DNA extraction, library preparation, and sequencing. Genomic DNA was extracted from cell pellets using overnight lysis in SDS with proteinase K at 37°C as previously described(70). Briefly, protein was precipitated with ammonium acetate and genomic DNA was precipitated with isopropanol. All the recovered genomic DNA was used as template for PCR to generate the sequencing libraries. The libraries were prepared as previously described (24). Illumina sequencing adapters were added using custom primers and sequencing was performed on the llumina NovaSeq 6000 PE150 platform at a depth of 5×10^7 reads per sample. Sequencing was performed by Novogene (Sacramento, CA).

CRISPR Screen Data analysis—Guide sequences were extracted from FASTQ files and matched to the Bassik library index using a custom R script. Raw counts for each guide were provided as input to the MAGECK algorithm (25). For the expansion screen, two replicates from plasmid DNA library were compared to 4 samples collected on day 23 (two from each donor). For the cytokine production screen, 4 samples collected on day 15 (two from each donor) were compared to 2 samples (1 from each donor) that were sorted for high cytokine expression. The MAGeCK algorithm was used to perform normalization, calculate log fold changes for guides and genes, and calculate adjusted *P* values.

Targeted CRISPR gene editing

Ribonucleoprotein (RNP) was prepared using synthetic sgRNA with 2'-O-methyl phosphorothioate modification (Synthego) diluted in TE buffer at 100 μM. 5 μl sgRNA was incubated with 2.5 μl Duplex Buffer (IDT) and 2.5 μg Alt-R S.p. Cas9 Nuclease V3 (IDT) for 30 minutes at room temperature. 100 μl reactions were assembled with 10 million T cells, 90 μl P3 buffer (Lonza), and 10 μl RNP. Cells were pulsed with protocol EO115 using the P3 Primary Cell 4D-Nucleofector Kit and *4D Nucleofector* System (Lonza). Cells were recovered immediately with warm media for 6 hours prior to transduction with CAR. Guides sequences: AAVS1-sg1 5' GGGGCCACUAGGGACAGGAU 3', CCNC-sg40 5' GAUGCCAAAAACACACAUGU 3', CCNC-sg46 5' GGAUUUAAAGUUUCUCUCAG 3', MED12-sg48 5' CCUGCCUCAGGAUGAACUGA 3', MED12-sg49 5' UAACCAGCCUGCUGUCUCUG 3'.

Assessment of targeted CRISPR gene editing

4–7 days after editing, genomic DNA was extracted with QuickExtract DNA Extraction Solution (Lucigen) and ~500 bp regions flanking the cut site were amplified with Phusion Hot Start Flex 2X Master Mix (New England Biolabs) according to manufacturer's instructions. Sanger sequencing traces were analyzed by Inference of CRISPR Editing (ICE) (31).

Cell lines

NALM-6 leukemia cells and 143B osteosarcoma cells were obtained from American Type Culture Collection. Cell lines were stably transduced with GFP and firefly luciferase. Nalm6-GD2 was engineered to stably express GD2 synthase and GD3 synthase to obtain surface expression of GD2 disialoganglioside. Single cell clones were selected for high expression of GFP, luciferase, and GD2. Cell lines were maintained in RPMI (Gibco) supplemented with 10 mM HEPES, 10% FBS, and 1X penicillin-streptomycin-glutamine supplement (Gibco).

T cell expansion and viability assays

T cells were activated for 4 days at a 1:3 ratio of T cells to anti-CD3/28 Dynabeads (Invitrogen). T cell expansion assays were performed with IL-2 in the culture medium at 10 ng/mL (21.8 IU/mL) unless indicated otherwise. Cell counts and viability measurements were obtained using the Cellaca Mx Automated Cell Counter (Nexcelom). Cells were stained with acridine orange and propidium iodide to assess viability. A portion of the culture volume was discarded at each passage and the fraction of cells maintained in culture was used to calculate total cell counts.

CDK8 kinase inhibitor assays

SEL120 (SEL120–34A) hydrochloride, AS2863619, and CCT251545 (Selleckchem) were reconstituted at 5 mM in DMSO and stored at −80°C. Human primary T cells were plated in 96 well plates with 50,000 T cells per well. Inhibitors were added 24 hours after CD3/CD28 bead activation and were freshly supplemented every 48 hours. CD3/28 beads were removed on day 4 following activation. The reported IC50 for CDK8 is 4.4 nM, 0.6 nM, and 5 nM for SEL120, AS286319, and CCT251545, respectively. The IC50 for CDK19 is 10.4 nM, 4.3 nM, and 6.3 for SEL120, AS286319, and CCT251545, respectively.

Serial stimulation assay

Starting from 10 days post-activation, CAR-T cells were plated at a 1:1 ratio with GFP^+ tumor cells without IL-2. At 48–72 hour intervals, cell counts were recorded, and flow cytometry was performed to assess the ratio of T cells to tumor cells. Co-cultures were then collected and replated in fresh media and additional tumor cells were added to maintain a 1:1 effector to target ratio.

Cytokine production assays

5×10^4 T cells and 5×10^4 tumor cells were co-cultured in 250 μl media without IL-2 in round bottom 96 well plates for 24 hours. Culture supernatants were collected and analyzed by ELISA. IL-2 and IFNγ were detected with the ELISA MAX kit (Biolegend) and TNF-alpha was detected with the Quantikine kit (R&D Systems). Bead-based multiplex cytokine detection assays were performed at the Human Immune Monitoring Center (Stanford University) using the Luminex platform. Non-transduced T cells, which were CD3/28 activated but not retrovirally transduced or gene-edited, were included as a negative control.

Incucyte cytotoxicity assay

5×10^4 tumor cells were co-cultured with variable numbers of CAR-T cells in 250 μl media without IL-2 in flat bottom 96 well plates for 80 hours. Time lapse microscopy images were obtained with the Incucyte Live Cell Analysis system (Essen Bioscience) at 10X magnification. Total green object integrated intensity (GCU x μm^2/image) was used to assess tumor killing. Effector to target cell ratios are indicated in the figures or figure legends.

RT-qPCR

RNA was extracted with RNeasy kit (Qiagen) and cDNA was synthesized with High-Capacity cDNA Reverse Transcription kit (ThermoFisher). RT-qPCR was performed with PowerUp SYBR Green Master Mix (ThermoFisher) using the Bio-Rad CFX thermocycler and CFX Manager software. Target gene expression was normalized to the 18S housekeeping gene using the 2ΔΔCt method. IFNG-F 5' TGACCAGAGCATCCAAAAGA 3', IFNG-R 5' CTCTTCGACCTCGAAACAGC 3', IL2-F 5' TGCATTGCACTAAGTCTTGCAC 3', IL2-R 5' AGTTCTGTGGCCTTCTTGGG 3', TNF-F 5' CACAGTGAAGTGCTGGCAAC 3', TNF-R 5' AGGAAGGCCTAAGGTCCACT 3', 18S-F 5' GCAGAATCCACGCCAGTACAAG 3', 18S-R 5' GCTTGTTGTCCAGACCATTGG 3'.

Seahorse Assay

Metabolic analysis was carried out using Seahorse Bioscience Analyzer XFe96. Briefly, 2×10^6 cells were resuspended in XF assay media supplemented with 25 mM glucose, 2mM glutamine and 1 mM sodium pyruvate and plated on a Cell-Tak (Corning)-coated microplate allowing the adhesion of CAR T cells. Mitochondrial stress and glycolytic parameters were measured *via* oxygen consumption rate (OCR) (pmol/min) and extracellular acidification rate (ECAR) (mpH/min), respectively, with use of real-time injections of oligomycin (1.5 μM), carbonyl cyanide-*4* (trifluoromethoxy) phenylhydrazone (FCCP; 1 μM) and rotenone and antimycin (both 1 μM). Respiratory parameters were calculated following manufacturer's instructions (Seahorse Bioscience). All chemicals were purchased from Agilent unless stated otherwise.

Flow Cytometry

T cells were washed in FACS buffer (DPBS no calcium, no magnesium (Gibco) with 2% FBS). Cells were incubated on ice in FACS buffer with antibodies specific for cell surface markers for twenty minutes. Antibodies used are in Table S4. For pSTAT5 staining: cells were prepared with the Fix and Perm Cell Permeabilization kit (ThermoFisher) according to manufacturer's instructions. For pS6 staining: T cells were cultured 24 hours in complete AIM-V media without IL-2 prior anti-idiotype stimulation (1ug/ml of mouse IgG anti-human CD19 idiotype crosslinked with 10ug/ml of anti-mouse Fab in PBS). Cells were incubated with anti-idiotype - or left unstimulated - for 1 hour at 37C and kept on ice immediately afterwards. Cells were fixed (BD Phosphoflow Fix Buffer I) and then permeabilized (BD Perm Buffer III) following manufacturer's instructions. For mitochondrial mass staining: cells were stained with MitoTracker Green (Cell Signaling

Technology) at 200 nM, 37°C for 30 minutes. Prior to acquisition, cells resuspended in FACS buffer and analyzed on a LSRFortessa (BD) with BD FACSDiva software.

Western Blotting

Total cell lysates were extracted in non-denaturing lysis buffer (150 mM NaCl, 50 mM Tris pH 8, 1% NP-40, 0.25% sodium deoxycholate with Halt Protease Inhibitor Cocktail (ThermoFisher Scientific). Chromatin-bound and soluble cellular fractions were prepared with cytoskeletal lysis buffer (10 mM PIPES-KOH (pH 6.8), 100 mM NaCl, 300 mM sucrose, 3 mM MgCl2, and Halt Protease Inhibitor Cocktail. Briefly, cells were washed in PBS, resuspended in lysis buffer, and incubated on ice for 20 minutes. Cells were centrifuged at 5,000 rpm to separate the soluble and chromatin bound fractions. The soluble fraction was cleared by centrifugation at 13,000 rpm. The chromatin-bound fraction was resuspended in Sample Reducing Buffer (Pierce) and incubated at 100°C for 5 minutes. Protein concentration was assessed with the DC Protein Assay kit (Bio-Rad) and 20 μg total protein was loaded per sample. Equal volumes of soluble and chromatin fractions were loaded for each sample. SDS-PAGE electrophoresis was performed, and proteins were transferred to PVDF membranes for immunoblotting. Antibodies used are listed in Table S4. Immunofluorescence was detected with the Odyssey Imaging System (Licor), or chemiluminescence was detected with autoradiography film.

Western Blot Quantification

Images captured with autoradiography film were scanned at 600 dpi in 16-bit greyscale, and images captured with the Odyssey Imaging System were exported as JPEGs. Quantification was performed with ImageJ software. A region of interest (ROI) of equal size was used to measure the specific band and background signal in each lane. Pixel densities were subtracted from 255 to invert the image and the background values were subtracted from band values to adjust for background signal. For each sample, the background adjusted MED1 pixel density was divided by the same value from the HIST3 loading control to calculate a ratio of MED1 to HIST3. Ratios from donor 1 and donor 2 were normalized to the largest ratio collected in each independent experiment.

Mice

Immunocompromised NOD *scid* IL2Rgamma^{null} (NSG, Strain #005557) mice were purchased from JAX and bred in-house under sterile conditions. Mice were monitored daily by the Veterinary Service Center staff. Care and treatments were in compliance with Stanford University APLAC protocols. Leukemia cells and CAR-T cells were administered via intravenous injection. 143B osteosarcoma cells were administered by intramuscular injection. For some experiments, tumor burden was assessed prior to treatment and mice were randomized to groups to ensure equal tumor burden between treatment groups. Time of treatment and dosing is indicated in figure legends. Researchers were blinded during administration of T cells. Leukemia progression was monitored using the Lago SII (Spectral Instruments Imaging). Quantification of bioluminescence was performed with Aura software (Spectral Instruments Imaging). Solid tumor progression was followed using caliper measurements of the injected leg area. Researchers were blinded to the treatment groups during solid tumor measurements. Mice were euthanized upon manifestation of

paralysis, impaired mobility, poor body condition (score of BC2-), or when tumor diameter exceed 17 mm. Sample sizes of 5 mice per group were selected based on previous experience with these models. All experiments were repeated twice with different donors, and donors used for *in vivo* experiments were different from the screening experiments.

Blood Analysis

Blood was collected from the retro-orbital sinus into Microvette blood collection tubes with EDTA (Fisher Scientific). Whole blood was labeled with anti-CD45 (HI30, ThermoFisher) and red blood cells were lysed with FACS Lysing Solution (BD) according to manufacturer's instructions. Samples were mixed with CountBright Absolute Counting beads (ThermoFisher) prior to flow cytometry analysis.

CyTOF sample preparation and data analysis

2×10^6 CAR-T cells were washed in PBS and resuspended in 250 nM cisplatin (Fluidigm) for 3 minutes. Cells were washed twice in cell staining medium (CSM, PBS with 0.05% BSA and 0.02% sodium azide) followed by fixing in 1.6% paraformaldehyde for 10 minutes at room temperature. Cells were washed twice in PBS, flash frozen on dry ice, and stored at −80°C. Cells were thawed, washed in CSM, and barcoded with the Cell-ID 20-plex kit (Fluidigm) as previously described (71). Samples were pooled and stained for cell surface markers for 30 minutes at room temperature. Panel of antibodies can be found in Supplemental Table 3. CARs were detected with anti-idiotype antibodies conjugated to metals. The NY-ESO-1 TCR was detected with PE labeled tetramers, followed by 30 minutes of secondary staining with anti-PE-156Gd (Fluidigm). Intracellular staining was performed using Permeabilization buffer (eBioscience) for 45 minutes on ice followed by two CSM washes. Cells were resuspended with Cell-ID Intercalator-ID (Fluidigm), washed twice in deionized water, resuspended in 1X EQ beads, and acquired on a Helios mass cytometer (Fluidigm). After acquisition, data was normalized using MATLAB-based software (72) and debarcoded using MATLAB-debarcoder. Fsc files were uploaded to the OMIQ platform for analysis (OMIQ.ai).

Bulk RNA-seq

CAR-T cells were collected on day 15 and processed without freezing. RNA was extracted using the RNeasy mini kit (Qiagen). RNA quality was assessed by BioAnalyzer (Agilent). Sequencing libraries were prepared by Novogene (Sacramento, CA) and 150 bp paired end sequencing at a depth of 3×10^7 reads per sample was obtained using the Illumina NovaSeq6000 platform. FASTQ files were generated by Novogene. Transcripts were quantified with Salmon and DESeq2 was used to identify differentially expressed genes. GSEA analysis was performed using GSEA software (Broad Institute).

ChIP-seq

ChIP-seq was performed as previously described with minor modifications (73). CAR-T cells (3×10^6) were double crosslinked by 50mM DSG (disuccinimidyl glutarate, #C1104 - ProteoChem) for 30 minutes followed by 10 minutes of 1% formaldehyde. Formaldehyde was quenched by the addition of glycine. Nuclei were isolated with ChIP lysis buffer

(1% Triton x-100, 0.1% SDS, 150 mM NaCl, 1mM EDTA, and 20 mM Tris, pH 8.0). Nuclei were sheared with Covaris sonicator using the following setup: Fill level – 10, Duty Cycle – 5, PIP – 140, Cycles/Burst – 200, Time – 4 minutes). Sheared chromatin was immunoprecipitated overnight with the antibodies shown in Table 1. Antibody chromatin complexes were pulled down with Protein A magnetic beads and washed once in IP wash buffer I. (1% Triton, 0.1% SDS, 150 mM NaCl, 1 mM EDTA, 20 mM Tris, pH 8.0, and 0.1% NaDOC), twice in IP wash buffer II. (1% Triton, 0.1% SDS, 500 mM NaCl, 1 mM EDTA, 20 mM Tris, pH 8.0, and 0.1% NaDOC), once in IP wash buffer III. (0.25 M LiCl, 0.5% NP-40, 1mM EDTA, 20 mM Tris, pH 8.0, 0.5% NaDOC) and once in TE buffer (10 mM EDTA and 200 mM Tris, pH 8.0). DNA was eluted from the beads by vigorous shaking for 20 minutes in elution buffer (100mM $NaHCO_3$, 1% SDS). DNA was decrosslinked overnight at 65C and purified with MinElute PCR purification kit (Qiagen). DNA was quantified by Qubit and 10 ng DNA was used for sequencing library construction with the Ovation Ultralow Library System V2 (Tecan) using 12 PCR cycles. Libraries were sequenced on the llumina NovaSeq 6000 PE150 platform at a depth of 3×10^7 reads per sample.

ATAC-seq

Approximately 100k CAR-T cells were used from each sample. Nuclei were isolated with ATAC-LB (10mM Tris-HCl pH7.4, 10mM NaCl, 3mM MgCl2, 0.1% IGEPAL) and used for tagmentation using Nextera DNA Library Preparation Kit (Illumina) from three donors. After tagmentation DNA was purified with MinElute PCR Purification Kit (Qiagen). Tagmented DNA was then amplified with Phusion high-fidelity PCR master mix (NEB) using 14 PCR cycles. Amplified libraries were purified again with MinElute PCR Purification Kit. Fragment distribution of libraries was assessed with Agilent Bioanalyzer and libraries were sequenced on the llumina NovaSeq 6000 PE150 platform at a depth of 3×10^7 reads per sample. Sequencing was performed by Novogene (Sacramento, CA).

ATAC-seq and ChIP-seq data processing

Quality control, aligning, and signal tracks—Paired end fastq files were trimmed to remove adapters and low quality sequences using `fastp` and then were aligned to the hg38 reference genome using `hisat2` with the `--no-spliced-alignment` and `--very-sensitivè options. Duplicates were marked and removed with `picard MarkDuplicates.` Reads with high quality concordant alignments to human chromosomes chr1-chr22 and chrX (e.g., excluding chrY and chrM) were converted to BED files for downstream processing. Bigwig files were normalized by using the number of fragments overlapping peaks genome wide, which controls for differences in sequencing depth and also library quality between samples, were exported from R using `rtracklayer::export` and visualized using the Integrative Genomics Viewer (IGV). Plots were generated in R using ChIPpeakAnno (3.13)(74).

Obtaining a union peak set and counts matrix—Peaks were called for each replicate using MACS2. Reproducible peaks for each sample were determined as peaks present in at least 2 of 3 replicates and merged to create a disjoint peak set for each sample. Reproducible peaks for each sample were then merged into a disjoint union peak set encompassing all samples using our previously described iterative procedure which merges the peak sets

by repeatedly removing less significant overlapping peaks until no overlaps remain. The peak by sample counts matrix was obtained by counting reads overlapping with each peak. The counts matrix was loaded into DESeq2 for differential analysis. Selected peak sets were also visualized across samples by using the bigwig track files described above with `plotHeatmap` from the `deepTools` analysis suite.

Details of peak sets—Differential “up” and “down” peak sets: obtained from DESeq2 pairwise comparisons using FDR >= 0.05 and sometimes an additional fold change threshold, as indicated. “Bound” peak sets: for each sample (where a sample is, for example “h3k27ac_MED12_unstim”) bound peaks were determined based on thresholding the normalized counts matrix. The normalized counts matrix was obtained by multiplying each column (replicate) in the counts matrix by (1e6 / total reads in peaks in that replicate). The bound peaks for each sample were then determined as peaks which had at least 2 of 3 replicates with a normalized value greater than a threshold. A cutoff of 2 was selected empirically, which yielded between 60,000 and 120,000 peaks per sample. Finally, bound peak sets for each sample were merged into bound peak sets for each sample set (e.g., an overall h3k27ac CAR-T peak set) by taking the union.

Motif analysis—Motifs enriched in particular peak sets were analyzed using the HOMER `findMotifsGenome.pl` utility or chromVAR for ATAC-seq samples. For HOMER analysis, total bound peaks for each sample set were used as background, thus, the enrichments represent motif enrichments relative to general CAR-T specific peaks rather than enrichments relative to the whole genome.

Single-cell RNA-seq

Isolation of tumor infiltrating NY-ESO-1$^+$ T cells—Tumors were harvested 6 days after adoptive transfer of NY-ESO-1$^+$ T cells. Tissue dissociation was performed with the Mouse Tumor Dissociation Kit (Miltenyi) and Gentle MACS C tubes (Miltenyi) according to manufacturer’s instructions. Red blood cells were lysed (Red Blood Cell Lysis Solution, Miltenyi), and samples were washed and passed through 70 μm filters prior to staining for 30 minutes at room temperature with fixable viability dye eFluor506 (eBioscience), antibodies specific for Vβ13.1, the beta chain of the NY-ESO-1 TCR (Table S4), and tetramers loaded with the SLLMWITQC peptide. Cell sorting of live, tetramer$^+$, Vβ13.1$^+$ cells was performed at the Stanford Shared FACS Facility on a FACSAria II equipped with a 70μm nozzle.

scRNA-seq Library Preparation and Sequencing—Cells harvested from 4 tumors from each experimental condition were pooled and capture was performed at the Stanford Function Genomics Facility using the 10X Genomics platform. Sequencing libraries were prepared with the 10X Chromium Next GEM Single Cell 3’ v 3.1 kit (10X Genomics) according to manufacturer’s instructions. Deep sequencing of single-index libraries was performed by Novogene (Sacramento, CA) on the llumina NovaSeq 6000 PE150 platform with an average depth of approximately 38,000 reads per cell.

scRNA-seq Data Processing and Analysis—Index demultiplexing and generation of FASTQ files was performed by Novogene. Alignment to hg38 was performed with Cell Ranger v7.0.0 (10X Genomics). Filtering was performed to remove debris and dead cells using the Seurat package v4.1.1 in R. Clustering of scRNA-seq profiles, dimensionality reduction using UMAP, and differential gene analysis was performed with Seurat. For comparison to published datasets, marker genes for each cluster of Zheng et al. were obtained from Table S3 of the Zheng et al. manuscript (41). For each cluster, the top 50 marker genes were obtained by using the effect size ranking (column “comb.ES.rank” in Zheng et al. Table S3). A module score for each gene set was added to each cell in our TIL scRNA-seq dataset with the Seurat function ÀddModuleScorè and then visualized by genotype (MED12-sg49 vs Control sg1). Statistical significance was assessed via two-sided Wilcoxon test using R function `wilcox.test.`

Supplementary Material

Refer to Web version on PubMed Central for supplementary material.

Funding:

This work was supported by the National Institutes of Health U54CA232568-01 (C.L.M.), RM1-HG007735 (H.Y.C.), R35-CA209919 (H.Y.C.), U01CA260852 (A.T.S.); **a** Stand Up 2 Cancer–St. Baldrick’s–National Cancer Institute Pediatric Cancer Dream Team Translational Research Grant (SU2CAACR-DT1113, C.L.M.); Parker Institute for Cancer Immunotherapy (A.T.S., H.Y.C., and C.L.M.); Virginia and D.K. Ludwig Fund for Cancer Research (C.L.M.); Sponsored research award from Lyell Immunopharma (C.L.M.); The Burroughs Welcome Fund Career Award for Medical Scientists (A.T.S.); Pew-Stewart Scholars for Cancer Research Award (A.T.S.); **and the** Cancer Research Institute Lloyd J. Old STAR Award (A.T.S.). Stand Up 2 Cancer is a program of the Entertainment Industry Foundation administered by the American Association for Cancer Research. C.L.M., H.Y.C., and A.T.S. are members of the Parker Institute for Cancer Immunotherapy, which supports the Stanford University Cancer Immunotherapy Program. H.Y.C. is an Investigator of the Howard Hughes Medical Institute. E.W.W. is a member of the Parker Institute for Cancer Immunotherapy and was funded by a Parker Institute Bridge Scholar Award. R.G.M. is the Taube Distinguished Scholar for Pediatric Immunotherapy at Stanford University School of Medicine. J.A.B was supported by a Stanford Graduate Fellowship and the National Science Foundation Graduate Research Fellowship under Grant No. DGE-1656518. K.A.F. was supported by the National Science Foundation Graduate Research Fellowship under Grant No. DGE-1656518. Sorting was performed on an instrument in the Stanford Shared FACS Facility obtained using NIH S10 Shared Instrument Grant S10RR025518-01. Tetramers were obtained from The NIH Tetramer Facility which is supported by contract 75N93020D00005.

Data and materials Availability:

ATAC-seq, ChIP-seq, and RNA-seq data has been deposited into the Gene Expression Omnibus (GEO) repository under the accession number GSE174282. ATAC-seq and ChIP-seq data can be viewed through the UCSC Genome Browser at the following link: https://genome.ucsc.edu/s/kfreitas/med12%2Dcart%2Dv3

References and Notes

1. Maude SL et al. , Tisagenlecleucel in Children and Young Adults with B-Cell Lymphoblastic Leukemia. N. Engl. J. Med. 378, 439–448 (2018). [PubMed: 29385370]
2. Lee DW et al. , T cells expressing CD19 chimeric antigen receptors for acute lymphoblastic leukaemia in children and young adults: A phase 1 dose-escalation trial. Lancet. 385, 517–528 (2015). [PubMed: 25319501]
3. Ribas A, Wolchok JD, Cancer immunotherapy using checkpoint blockade. Science (80-.). 359, 1350–1355 (2018).

4. Majzner RG, Mackall CL, Clinical lessons learned from the first leg of the CAR T cell journey. Nat. Med. 25, 1341–1355 (2019). [PubMed: 31501612]
5. Locke FL et al. , Long-term safety and activity of axicabtagene ciloleucel in refractory large B-cell lymphoma (ZUMA-1): a single-arm, multicentre, phase 1–2 trial. Lancet Oncol. 20, 31–42 (2019). [PubMed: 30518502]
6. Rosenberg SA et al. , Treatment of patients with metastatic melanoma with autologous tumor-infiltrating lymphocytes and interleukin 2. J. Natl. Cancer Inst. 86, 1159–1166 (1994). [PubMed: 8028037]
7. Robbins PF et al. , Tumor regression in patients with metastatic synovial cell sarcoma and melanoma using genetically engineered lymphocytes reactive with NY-ESO-1. J. Clin. Oncol. 29, 917–924 (2011). [PubMed: 21282551]
8. D'angelo SP et al. , Antitumor activity associated with prolonged persistence of adoptively transferred NY-ESO-1c259 T cells in synovial sarcoma. Cancer Discov. 8, 944–957 (2018). [PubMed: 29891538]
9. Fraietta JA et al. , Determinants of response and resistance to CD19 chimeric antigen receptor (CAR) T cell therapy of chronic lymphocytic leukemia. Nat. Med. 24, 563–571 (2018). [PubMed: 29713085]
10. Philip M et al. , Chromatin states define tumour-specific T cell dysfunction and reprogramming. Nature. 545, 452–456 (2017). [PubMed: 28514453]
11. Srivastava S et al. , Immunogenic Chemotherapy Enhances Recruitment of CAR-T Cells to Lung Tumors and Improves Antitumor Efficacy when Combined with Checkpoint Blockade. Cancer Cell. 39, 193–208.e10 (2021). [PubMed: 33357452]
12. Anderson KG et al. , Obstacles Posed by the Tumor Microenvironment to T cell Activity: A Case for Synergistic Therapies. Cancer Cell. 31, 311–325 (2017). [PubMed: 28292435]
13. Lynn RC et al. , c-Jun overexpression in CAR T cells induces exhaustion resistance. Nature. 576, 293–300 (2019). [PubMed: 31802004]
14. Chen J et al. , NR4A transcription factors limit CAR T cell function in solid tumours. Nature. 567, 530–534 (2019). [PubMed: 30814732]
15. Labanieh L et al. , Enhanced safety and efficacy of protease-regulated CAR-T cell receptors. Cell. 185, 1745–1763.e22 (2022). [PubMed: 35483375]
16. Weber EW et al. , Transient rest restores functionality in exhausted CAR-T cells through epigenetic remodeling. Science (80-.). 372 (2021), doi:10.1126/science.aba1786.
17. Stadtmauer EA et al. , CRISPR-engineered T cells in patients with refractory cancer. Science (80-.). 367 (2020), doi:10.1126/science.aba7365.
18. Shifrut E et al. , Genome-wide CRISPR Screens in Primary Human T Cells Reveal Key Regulators of Immune Function. Cell. 175, 1958–1971 (2018). [PubMed: 30449619]
19. Wang D et al. , CRISPR Screening of CAR T Cells and Cancer Stem Cells Reveals Critical Dependencies for Cell- Based Therapies. Cancer Discov. 11, 1192–1211 (2021). [PubMed: 33328215]
20. Belk JA et al. , Genome-wide CRISPR screens of T cell exhaustion identify chromatin remodeling factors that limit T cell persistence. Cancer Cell, 1–19 (2022).
21. El Khattabi L et al. , A Pliable Mediator Acts as a Functional Rather Than an Architectural Bridge between Promoters and Enhancers. Cell. 178, 1145–1158.e20 (2019). [PubMed: 31402173]
22. Whyte WA et al. , Master transcription factors and mediator establish super-enhancers at key cell identity genes. Cell. 153, 307–319 (2013). [PubMed: 23582322]
23. Quevedo M et al. , Mediator complex interaction partners organize the transcriptional network that defines neural stem cells. Nat. Commun. 10, 1–15 (2019). [PubMed: 30602773]
24. Morgens DW et al. , Genome-scale measurement of off-target activity using Cas9 toxicity in high-throughput screens. Nat. Commun. 8, 1–8 (2017). [PubMed: 28232747]
25. Li W et al. , MAGeCK enables robust identification of essential genes from genome-scale CRISPR/Cas9 knockout screens. Genome Biol. 15, 554 (2014). [PubMed: 25476604]

26. Sabbagh L et al. , The Selective Increase in Caspase-3 Expression in Effector but Not Memory T Cells Allows Susceptibility to Apoptosis. J. Immunol. 173, 5425–5433 (2004). [PubMed: 15494489]
27. Majzner RG et al. , Tuning the Antigen Density Requirement for CAR T-cell activity. Cancer Discov. 10, 702–723 (2020). [PubMed: 32193224]
28. Verger A et al. , Twenty years of Mediator complex structural studies. Biochem. Soc. Trans. 47, 399–410 (2019). [PubMed: 30733343]
29. Abdella R et al. , Structure of the human Mediator-bound transcription preinitiation complex. Science (80-.). 3074, 1–11 (2021).
30. Li YC et al. , Structure and noncanonical Cdk8 activation mechanism within an Argonaute-containing Mediator kinase module. Sci. Adv. 7 (2021), doi:10.1126/sciadv.abd4484.
31. Hsiau T et al. , Inference of CRISPR Edits from Sanger Trace Data. bioRxiv, 1–17 (2018).
32. Long AH et al. , 4–1BB costimulation ameliorates T cell exhaustion induced by tonic signaling of chimeric antigen receptors. Nat. Med. 21, 581–590 (2015). [PubMed: 25939063]
33. Li N et al. , Cyclin C is a haploinsufficient tumour suppressor. Nat. Cell Biol. 16, 1080–1091 (2014). [PubMed: 25344755]
34. Moyo MB et al. , Altered chromatin landscape and enhancer engagement underlie transcriptional dysregulation in MED12 mutant uterine leiomyomas. Nat. Commun. 11, 1–16 (2020). [PubMed: 31911652]
35. Geltink RIK et al. , Unraveling the Complex Interplay between T Cell Metabolism and Function. Annu. Rev. Immunol. 36, 461–488 (2018). [PubMed: 29677474]
36. Levine LS et al. , Single-cell analysis by mass cytometry reveals metabolic states of early-activated CD8+ T cells during the primary immune response. Immunity. 54, 829–844.e5 (2021). [PubMed: 33705706]
37. Krishna S et al. , Stem-like CD8 T cells mediate response of adoptive cell immunotherapy against human cancer. Science (80-.). 370, 1328–1334 (2020).
38. Gupta PK et al. , CD39 Expression Identifies Terminally Exhausted CD8+ T Cells. PLoS Pathog. 11, 1–21 (2015).
39. Thomas R et al. , NY-ESO-1 based immunotherapy of cancer: Current perspectives. Front. Immunol. 9 (2018), doi:10.3389/fimmu.2018.00947.
40. Good CR et al. , An NK-like CAR T cell transition in CAR T cell dysfunction. Cell. 184, 6081–6100.e26 (2021). [PubMed: 34861191]
41. Zheng L et al. , Pan-cancer single-cell landscape of tumor-infiltrating T cells. Science (80-.). 374 (2021), doi:10.1126/science.abe6474.
42. Hamann D et al. , Phenotypical and functional separation of memory and effector human CD8+ T cells. J. Exp. Med. 186, 1407–1418 (1997). [PubMed: 9348298]
43. Romero P et al. , Four Functionally Distinct Populations of Human Effector-Memory CD8 + T Lymphocytes. J. Immunol. 178, 4112–4119 (2007). [PubMed: 17371966]
44. Sallusto F et al. , Two subsets of memory T lymphocytes with distinct homing potentials and effector functions. Nature. 401, 708–712 (1999). [PubMed: 10537110]
45. Muroyama Y, Wherry EJ, Memory T-Cell Heterogeneity and Terminology. Cold Spring Harb. Perspect. Biol, 1–20 (2021).
46. Joshi NS et al. , Inflammation Directs Memory Precursor and Short-Lived Effector CD8+ T Cell Fates via the Graded Expression of T-bet Transcription Factor. Immunity. 27, 281–295 (2007). [PubMed: 17723218]
47. Soutourina J, Transcription regulation by the Mediator complex. Nat. Rev. Mol. Cell Biol. 19, 262–274 (2018). [PubMed: 29209056]
48. Chen Z et al. , In vivo CD8 + T cell CRISPR screening reveals control by Fli1 in infection and cancer. Cell, 1–19 (2021). [PubMed: 33417857]
49. Delpoux A et al. , FOXO1 constrains activation and regulates senescence in CD8 T cells. Cell Rep. 34 (2021), doi:10.1016/j.celrep.2020.108674.
50. Kim HP et al. , Both integrated and differential regulation of components of the IL-2/IL-2 receptor system. Cytokine Growth Factor Rev. 17, 349–366 (2006). [PubMed: 16911870]

51. Liao W et al. , Modulation of cytokine receptors by IL-2 broadly regulates differentiation into helper T cell lineages. Nat. Immunol. 12, 551–559 (2011). [PubMed: 21516110]
52. Tripathi P et al. , STAT5 Is Critical To Maintain Effector CD8 + T Cell Responses. J. Immunol. 185, 2116–2124 (2010). [PubMed: 20644163]
53. Hand TW et al. , Differential effects of STAT5 and PI3K/AKT signaling on effector and memory CD8 T-cell survival. Proc. Natl. Acad. Sci. U. S. A. 107, 16601–16606 (2010). [PubMed: 20823247]
54. Verdeil G et al. , STAT5-Mediated Signals Sustain a TCR-Initiated Gene Expression Program toward Differentiation of CD8 T Cell Effectors. J. Immunol. 176, 4834–4842 (2006). [PubMed: 16585578]
55. Jansen CS et al. , An intra-tumoral niche maintains and differentiates stem-like CD8 T cells. Nature. 576, 465–470 (2019). [PubMed: 31827286]
56. Gattinoni L et al. , A human memory T cell subset with stem cell-like properties. Nat. Med. 17, 1290–1297 (2011). [PubMed: 21926977]
57. Vodnala SK et al. , T cell stemness and dysfunction in tumors are triggered by a common mechanism. Science (80-.). 363, 1–12 (2019).
58. Tsai KL et al. , A conserved Mediator-CDK8 kinase module association regulates Mediator-RNA polymerase II interaction. Nat. Struct. Mol. Biol. 20, 611–619 (2013). [PubMed: 23563140]
59. Knuesel MT et al. , The human CDK8 subcomplex is a molecular switch that controls Mediator coactivator function. Genes Dev. 23, 439–451 (2009). [PubMed: 19240132]
60. Wang X et al. , Structural flexibility and functional interaction of mediator Cdk8 module. Protein Cell. 4, 911–920 (2013). [PubMed: 24043446]
61. Aranda-Orgilles B et al. , MED12 Regulates HSC-Specific Enhancers Independently of Mediator Kinase Activity to Control Hematopoiesis. Cell Stem Cell. 19, 784–799 (2016). [PubMed: 27570068]
62. Galbraith MD et al. , CDK8 Kinase Activity Promotes Glycolysis. Cell Rep. 21, 1495–1506 (2017). [PubMed: 29117556]
63. Neumayr C et al. , Differential cofactor dependencies define distinct types of human enhancers. Nature. 606, 406–413 (2022). [PubMed: 35650434]
64. Wei SC et al. , Distinct Cellular Mechanisms Underlie Anti-CTLA-4 and Anti-PD-1 Checkpoint Blockade. Cell. 170, 1120–1133.e17 (2017). [PubMed: 28803728]
65. Kaech SM et al. , Selective expression of the interleukin 7 receptor identifies effector CD8 T cells that give rise to long-lived memory cells. Nat. Immunol. 4, 1191–1198 (2003). [PubMed: 14625547]
66. Wherry EJ et al. , Lineage relationship and protective immunity of memory CD8T cell subsets. Nat. Immunol. 4, 225–234 (2003). [PubMed: 12563257]
67. Firestein R et al. , CDK8 is a colorectal cancer oncogene that regulates β-catenin activity. Nature. 455, 547–551 (2008). [PubMed: 18794900]
68. Gilmore JD et al. , CRISPR-Cas9 In Vivo Gene Editing for Transthyretin Amyloidosis. N. Engl. J. Med, 1–10 (2021).
69. Ashmore-Harris C, Fruhwirth GO, The clinical potential of gene editing as a tool to engineer cell-based therapeutics. Clin. Transl. Med. 9 (2020), doi:10.1186/s40169-020-0268-z.
70. Yau EH, Rana TM, Next-generation sequencing of genome-wide CRISPR screens. Methods Mol. Biol. 1712, 203–216 (2018). [PubMed: 29224076]
71. Zunder ER et al. , Palladium-based mass tag cell barcoding with a doublet-filtering scheme and single-cell deconvolution algorithm. Nat. Protoc. 10, 316–333 (2015). [PubMed: 25612231]
72. Finck R et al. , Normalization of mass cytometry data with bead standards. Cytom. Part A 83 A, 483–494 (2013).
73. Daniel B et al. , “Mapping the genomic binding sites of the activated retinoid X receptor in murine bone marrow-derived macrophages using chromatin immunoprecipitation sequencing.” in Methods in Molecular Biology (2014), pp. 15–24.
74. Zhu LJ et al. , ChIPpeakAnno: A Bioconductor package to annotate ChIP-seq and ChIP-chip data. BMC Bioinformatics. 11 (2010), doi:10.1186/1471-2105-11-237.

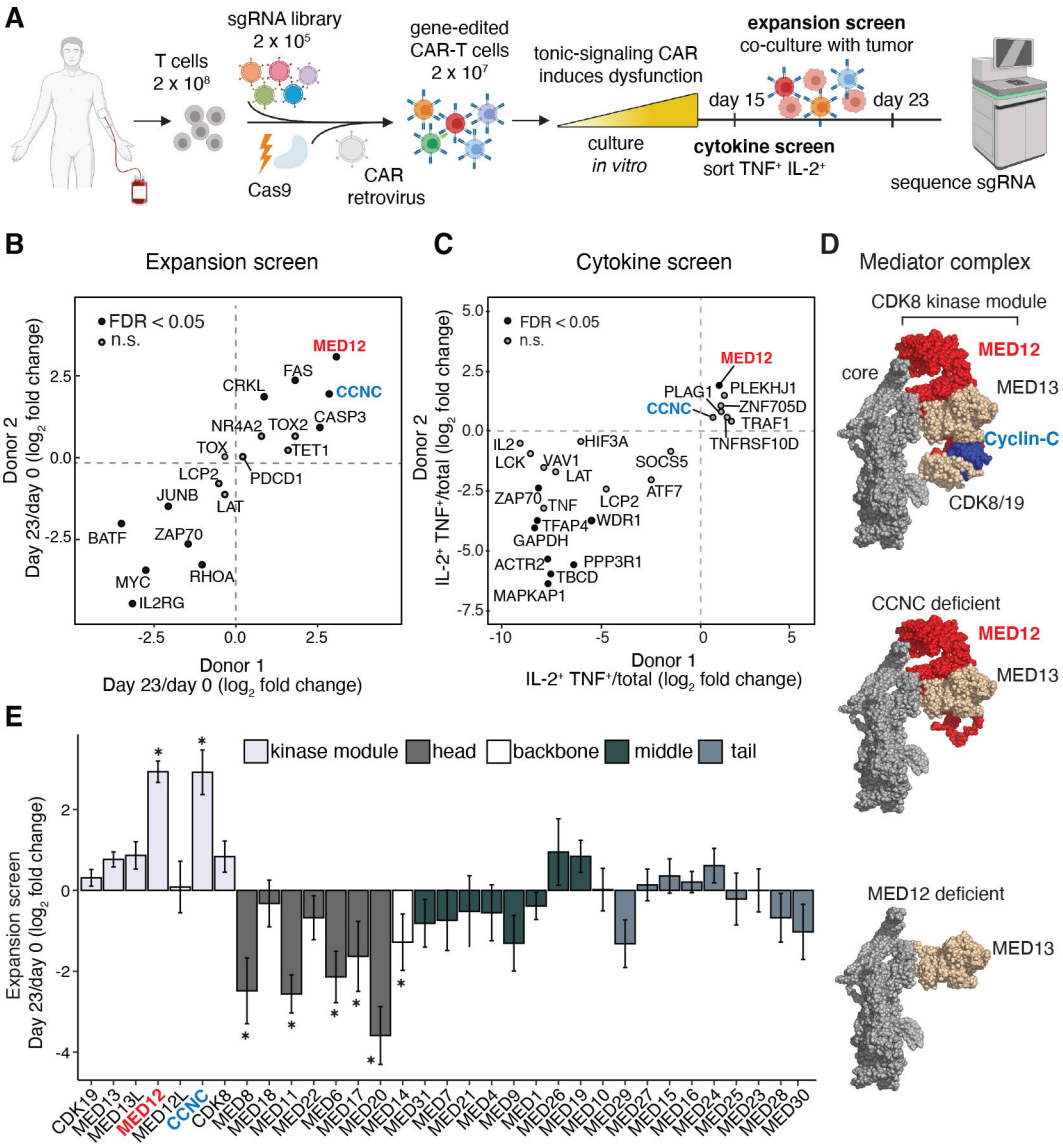

Fig. 1. Genome-wide CRISPR screen identifies subunits of the Mediator kinase module as regulators of CAR-T cell effector function.

A) Schematic depicting CRISPR knockout screen for regulators of cytokine production and CAR-T cell expansion using a tonic signaling model of CAR-T cell exhaustion.

B) Enrichment of gene knockouts in replicate expansion screens. CRISPR-edited HA-28ζ CAR-T cells were generated from two donors, cultured *in vitro* for 15 days, and then co-cultured with $GD2^+$ tumor cells until day 23.

C) Enrichment of gene knockouts in replicate cytokine production screens. CRISPR-edited HA-28ζ CAR-T cells were generated from two donors, cultured *in vitro* for 15 days, stimulated with $GD2^+$ tumor cells, and the top 10% of TNFα and IL-2 expressing cells were isolated by FACS.

D) Predicted Cryo-EM structure of yeast Mediator complex (top) showing the effect that depletion of Cyclin C (*CCNC* deficient) or *MED12* (*MED12* deficient) would have on assembly of other subunits. Core Mediator is shown in grey, CDK8 kinase module is

colored. Representations were created with Chimera using Protein Data Bank accessions 7KPX and 5U0P.

E) Bar graphs depicting enrichment of sgRNA targeting all Mediator complex subunits in the expansion screen. Data are mean ± s.d. (n = 4–10 guides per genes). Colors indicate module of the Mediator complex assigned to each subunit.

B, C, E) Data are mean of n = 4–10 guides per gene. Data are pooled from two independent experiments (n = 2 donors). Gene-level statistical significance was determined by the MAGeCK algorithm. *FDR < 0.05.

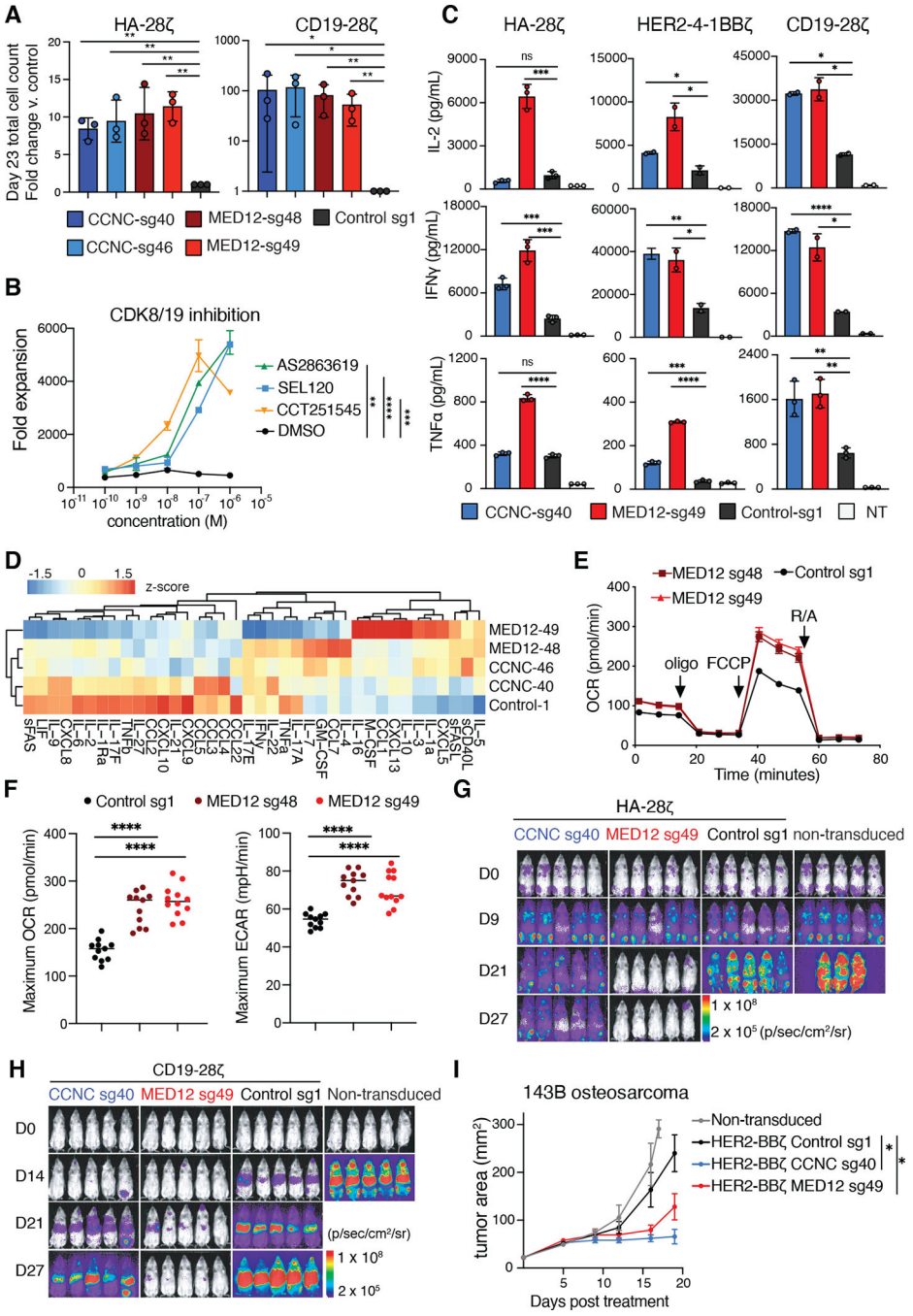

Fig. 2. Disruption of Mediator kinase module in CAR-T cells enhances T cell effector function and tumor clearance.

A) *In vitro* T cell expansion of *CCNC* and *MED12* deficient HA-28ζ (left) and CD19–28ζ (right) CAR-T cells. Fold change in total cell count after 23 days in culture relative to control CAR-T cells edited at the safe harbor AAVS1 locus. Two unique sgRNAs were used to validate each candidate gene. Data are mean ± s.d. of $n = 3$ donors. Ratio paired *t*-test. $*P < 0.05$, $**P < 0.01$.

B) *In vitro* expansion of human primary T cells with duals inhibitors of CDK8 and CDK19 over 15 days in culture. Inhibitors were supplemented to the media every 48 hours. Data are mean ± s.d of $n = 2$ replicate wells. Representative of 3 independent experiments.
C) IL-2 (top), IFNγ (middle), and TNFα (bottom) cytokine release after 24-hour co-culture with tumor cells from non-transduced (NT) and CAR-T cells edited with sgRNAs targeting *MED12*, *CCNC*, or safe-harbor control. HA-28ζ, CD19–28ζ and HER2–4-1BBζ CAR-T cells were stimulated 1:1 with NALM6-GD2, NALM6, or 143B cells respectively. Data are mean ± s.d. from duplicate or triplicate wells. Representative results of $n = 4$ donors (HA-28ζ, CD19–28ζ) or $n = 2$ donors (HER2–4-1BBζ). Non-transduced T cells were activated with CD3/28 stimulation, but not transduced with retrovirus or gene-edited.
D) Heatmap of 38 cytokines produced by control, *CCNC*, or *MED12* deficient CD19–28ζ CAR-T cells following 24-hour co-culture with NALM6 leukemia cells. Data are mean from duplicate wells in a multiplex bead-based assay. Two unique sgRNAs were used to validate each candidate gene.
E and F) Metabolic rate as measured by Seahorse analysis of oxygen consumption rate (OCR) and extracellular acidification rate (ECAR) of control or *MED12* deficient CD19–28ζ CAR-T cells under resting and challenge conditions. Data are mean of $n = 12$ replicate wells. Representative results from two independent experiments.
G) Analysis of tumor clearance. NSG mice were injected intravenously with 1.0×10^6 NALM6-GD2 leukemia cells and treated with 2.0×10^5 non-transduced or *CCNC* or *MED12* deficient HA-28ζ CAR-T cells 9 days after tumor infusion ($n = 5$ mice).
H) Analysis of tumor clearance. NSG mice were injected intravenously with 1.0×10^6 NALM6-Luc leukemia and treated with 2.5×10^5 non-transduced or *CCNC* or *MED12* deficient CD19–28ζ CAR-T cells 3 days after tumor infusion ($n = 5$ mice).
I) Analysis of tumor clearance. Tumor area of NSG mice injected intramuscular with 1×10^6 143B osteosarcoma cells and treated 4 days later with 5×10^6 non-transduced or *CCNC* or *MED12* deficient HER2–4-1BBζ CAR-T cells. Data are mean ± s.d of $n = 5$ mice (non-transduced, *MED12* and *CCNC* deficient) or $n = 4$ mice (Control). Two-way ANOVA test with Dunnett's multiple comparison test. $*P < 0.01$.
G, H, and I) Representative experiment from two independent experiments ($n = 2$ donors).
B, C and F) Two-tailed unpaired Student's *t*-test. $*P < 0.05$, $**P < 0.01$, $***P < 0.001$, $****P < 0.0001$

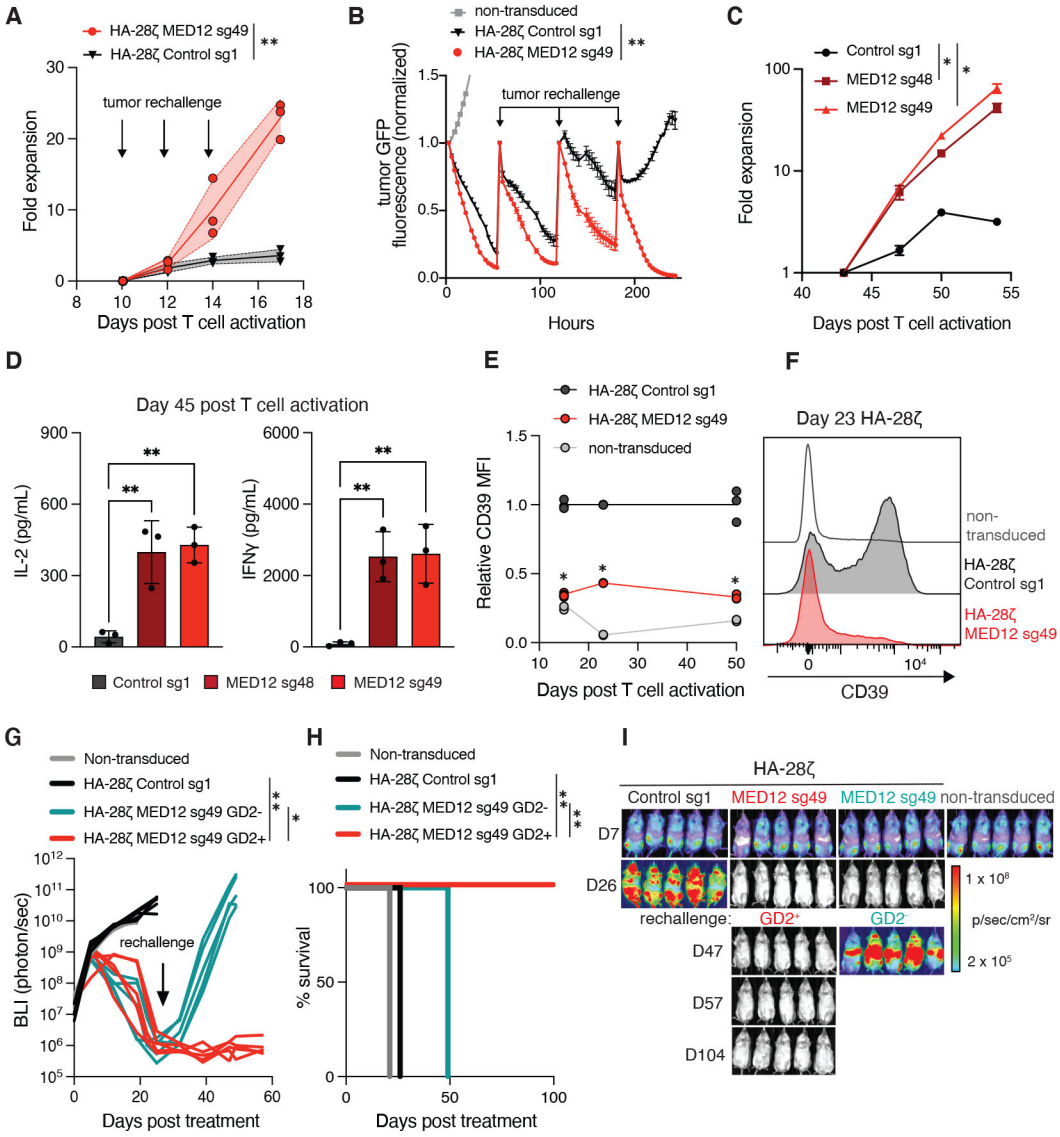

Fig. 3. Loss of *MED12* sustains effector function during chronic stimulation.

A) Antigen-driven *in vitro* expansion of Control and *MED12* deficient HA-28ζ CAR-T cells. CAR-T cells were serially stimulated with $GD2^+$ tumor cells in the absence of IL-2 at 48hr intervals at 1:1 effector to target cell ratio. Data are mean ± s.d. of $n = 3$ donors.

B) Cytotoxicity of Control and *MED12* deficient HA-28ζ CAR-T cells against GFP^+ NALM6-GD2 leukemia following serial stimulation beginning 10 days after T cell activation. Cells were counted and replated at a 1:1 ratio of T cells to tumor cells at 48–72-hour intervals in media without IL-2. Data are mean ± s.d. of $n = 3$ replicate cultures. Representative of 3 independent experiments.

C) *In vitro* expansion of Control and *MED12* deficient HA-28ζ CAR-T cells cultured with IL-2. Two unique sgRNAs were used to validate each candidate gene. Data are mean ± s.d. of $n = 2$ replicate cultures.

D) IL-2 (left) and IFNγ (right) release after 24-hour co-culture with tumor cells 45 days after T cell activation. Control and *MED12* deficient HA-28ζ CAR-T cells were stimulated 1:1 with NALM6-GD2. Data are mean ± s.d. from $n = 3$ replicate cultures.

E and F) Flow cytometric analysis of CD39 expression in non-transduced or HA-28ζ CAR-T cells. Mean fluorescence intensity is normalized to the Control at each timepoint. Data are mean ± s.d. of $n = 3$ replicate wells. Statistical comparison is between Control and MED12 deficient CAR-T cells.

G and I) Analysis of tumor clearance. Bioluminescent imaging (BLI) of NSG mice injected intravenously with 1×10^6 Nalm6-GD2 leukemia and treated with 4×10^5 non-transduced or *HA*-28ζ CAR-T cells 7 days after tumor infusion and rechallenged 26 days later with Nalm6 or Nalm6-GD2 cells ($n = 5$ mice).

H) Survival of CAR-treated mice shown in (G). Survival curves were compared with the Log-rank Mantel-Cox test. $*P < 0.01$.

A-D) Two-tailed unpaired Student's *t*-test. $*P < 0.05$, $**P < 0.01$.

E and G) Two-way ANOVA test with Dunnett's multiple comparison test. $*P < 0.01$.

C - H) Representative of two independent experiments.

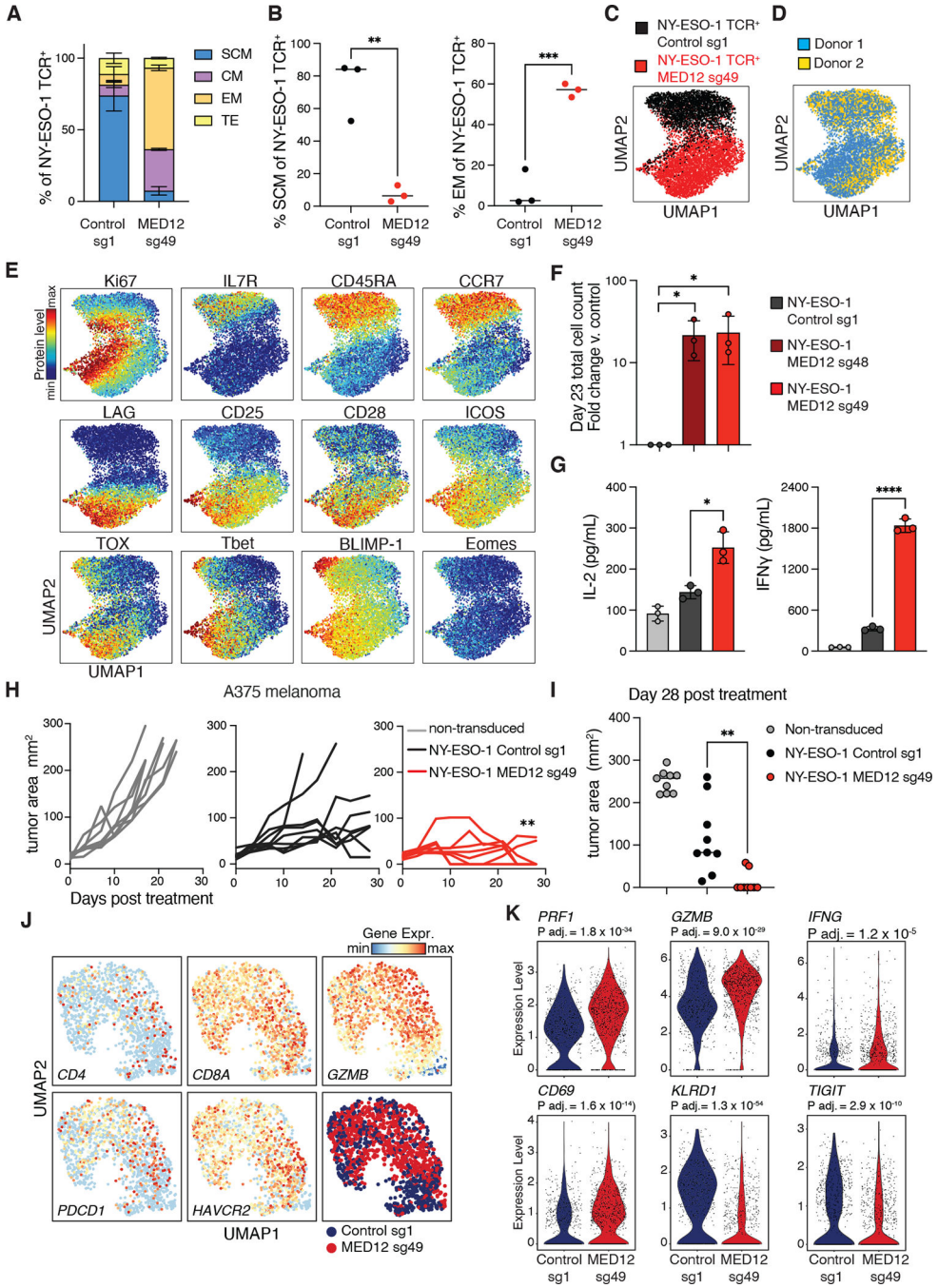

Fig. 4. Loss of *MED12* in T cells utilizing a TCR for tumor recognition enhances anti-tumor activity and effector function.

A and B) Frequency of T effector memory cells (CD45RO$^+$, CCR7$^-$) and stem cell memory (CCR7$^+$, CD45RO$^-$) in NY-ESO-1 TCR$^+$ cells 15 day after T cell activation. Data are mean ± of $n = 3$ donors. Two-tailed paired Student's *t*-test. $^{**}P < 0.01$, $^{***}P < 0.001$.

C-E) UMAP analysis of control and *MED12* deficient NY-ESO-1 TCR$^+$ cells. Expression of 34 markers was analyzed by CyTOF. Control and *MED12* deficient samples are combined

and colored C) by genotype, D) by donor, or E) by marker intensity. Each dot represents a single cell (n = 8319 cells). Data are pooled from two donors.

F) *In vitro* expansion of Control and *MED12* deficient NY-ESO-1 T cells cultured with IL-2. Data are mean ± s.d. of n = 3 donors.

G) IL-2 (left) and IFNγ (right) release after 24-hour co-culture of NY-ESO-1 T cells with A375 melanoma cells. Data are mean ± s.d. from n = 3 cultures. Representative of 3 independent experiments.

H and I) Analysis of tumor clearance. Tumor area of NSG mice injected subcutaneously with 3×10^6 A375 melanoma cells and treated 7 days later with 3×10^6 NY-ESO-1 TCR^+ cells. Tumor area was measured by caliper. H) One-way ANOVA test with Dunnett's multiple comparison test, $*P < 0.01$. I) Two-tailed unpaired Student's t-test, $**P < 0.01$. n = 9 mice pooled from two independent experiments.

J) scRNA-seq profiles of NY-ESO-1 TCR^+ T cells isolated from A375 melanoma tumors by FACS. T cells were administered 12 days following tumor engraftment, and tumors were harvested 6 days after treatment. Each dot represents a single cell and is colored by gene expression of the indicated genes or by genotype. Data are n = 1542 single cells pooled from 4 tumors from each genotype.

K) Violin plots depicting transcript expression level of selected genes in NY-ESO-1^+ tumor infiltrating T cells. n = 669 Control sg1 cells and 855 MED12 sg49 cells. Boxes indicate median and interquartile ranges.

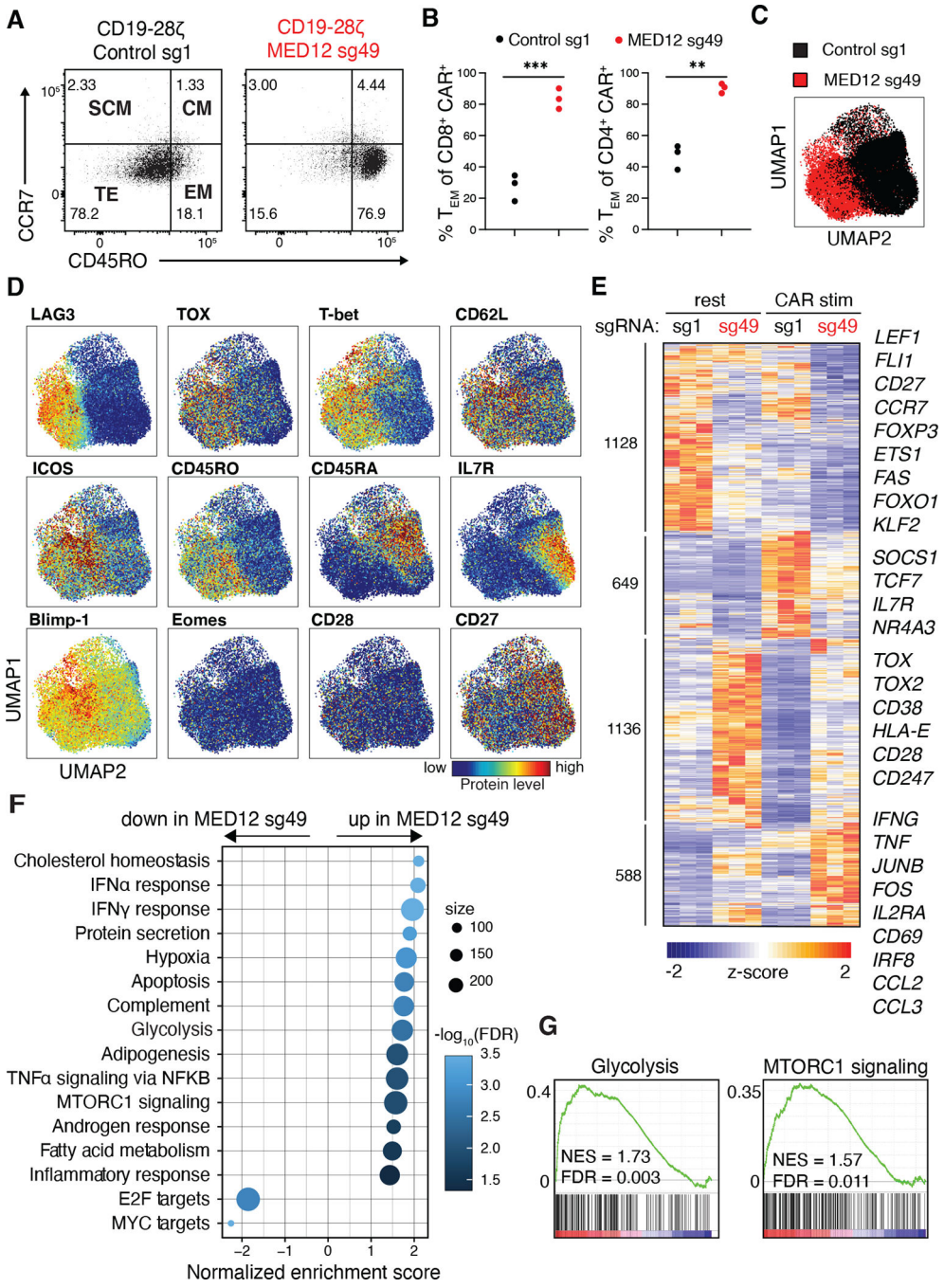

Fig. 5. *MED12* deficient CD19–28ζ CAR-T cells have an effector-like phenotype and an activated transcriptional program.

A) Flow cytometry analysis of T cell subsets as assessed by CD45RO and CCR7 expression in control or *MED12* deficient CD8$^+$ CD19–28ζ CAR-T cells 23 days after T cell activation. Representative result of $n = 3$ donors. Gating and subtyping strategy shown (SCM, Stem Central Memory; CM, Central Memory, TE, Terminal Effector; EM, Effector Memory)

B) Frequency of T effector memory cells (CD45RO$^+$, CCR7$^-$) in CD8$^+$ and CD4$^+$ CAR-T cells. $n = 3$ donors. Two-tailed paired Student's *t*-test. $^{**}P < 0.01$, $^{***}P < 0.001$.

C and D) Uniform Manifold Approximation and Projection (UMAP) analysis of control and *MED12* deficient CD19–28ζ CAR-T cells 15 days after T cell activation. Expression of 34 markers was analyzed by CyTOF. Control and *MED12* deficient samples are combined and colored **C)** by genotype or **D)** by marker intensity. Representative donor of $n = 3$ donors. Each dot represents a single cell ($n = 30{,}000$ cells).

E) Heatmap of differentially expressed genes in control or *MED12* deficient CD19–28ζ CAR-T cells detected by bulk RNA-seq 15 days after T cell activation. Cells were collected on day 15 and CAR stimulated for 3 hours with plate-bound anti-idiotype antibody. Adjusted $P < 0.01$. $n = 3$ donors.

F and G) Gene Set Enrichment Analysis of unstimulated *MED12* deficient CAR-T cells compared to control cells using the Hallmarks gene collection. Normalized Enrichment Scores (NES) and FDR q values are shown. A positive NES indicates the gene set was enriched in *MED12* deficient cells.

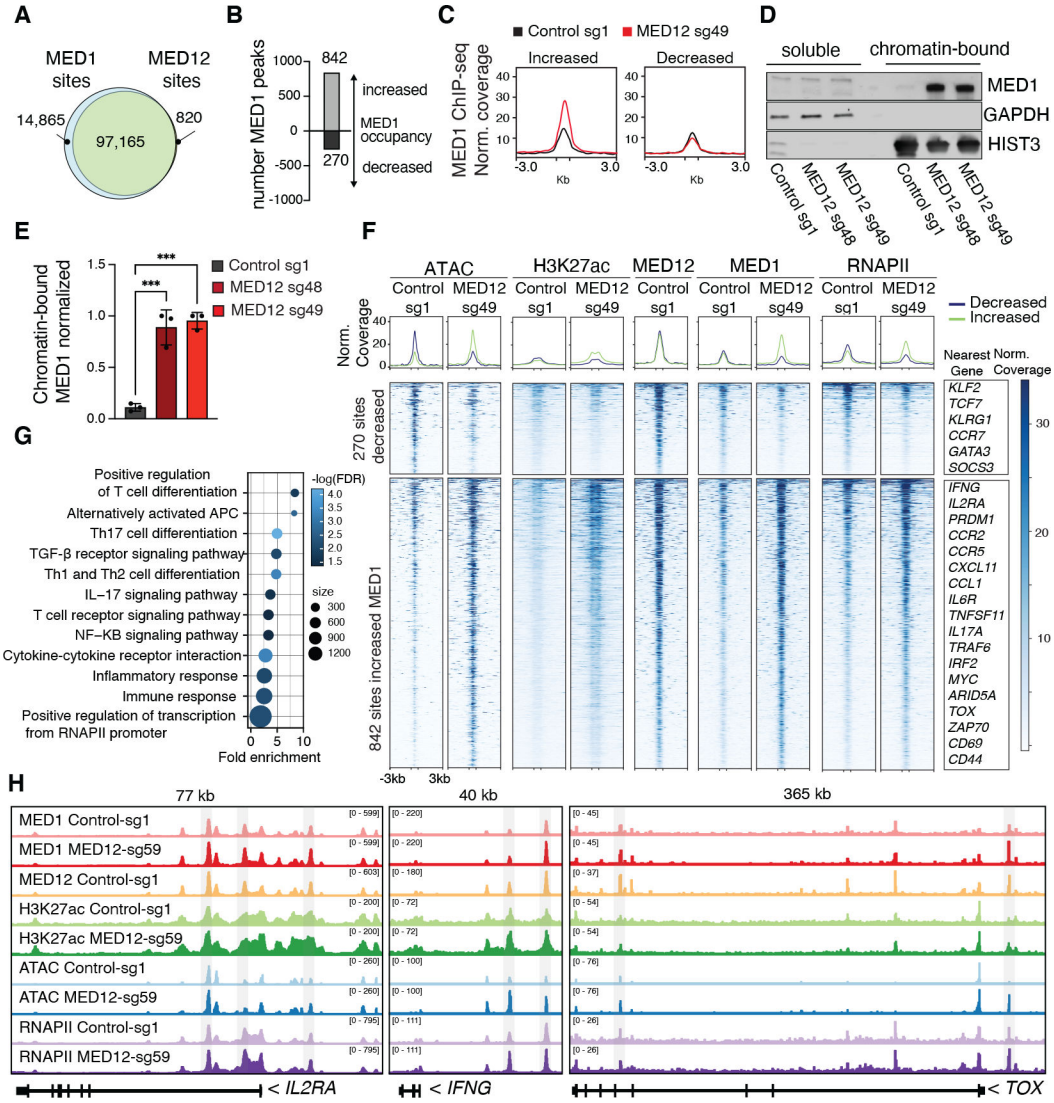

Fig. 6. Loss of *MED12* increases MED1 chromatin occupancy at transcriptionally active enhancers regulating T cell differentiation.

A) Venn diagram depicting number of sites bound by MED1 and/or MED12 detected by ChIP-seq in CD19–28ζ control CAR-T cells.

B) Number of genomic regions with significant change in MED1 occupancy detected by ChIP-seq between *MED12* deficient and control cells. Adjusted $P < 0.05$.

C) Mean normalized ChIP-seq signal at regions with significant differences in MED1 occupancy.

D) Western blot analysis of MED1 protein present in soluble and chromatin-bound cellular fractions from control and *MED12* deficient CD19–28ζ CAR-T cells 15 days after T cell activation. GAPDH and Histone 3 are used as markers for each cellular fraction. Representative blot from three independent experiments.

E) Densitometric analysis of western blot shown in (D). MED1 staining in the chromatin-bound fraction was normalized to HIST3 staining. Data are mean ± s.d. of $n = 3$ donors. Two-tailed unpaired Student's *t*-test. ***$P < 0.001$.

F) Heatmap showing ATAC-seq or ChIP-seq coverage at sites with differential MED12 occupancy as defined in (B).

G) DAVID functional annotation of 842 genes nearest to sites with increased MED1 occupancy in *MED12* deficient cells compared with control cells. 12 selected terms of 22 significant terms are shown (FDR < 0.10). Full results table including MED1 ChIP-seq coverage at genes corresponding to GO terms is included in Supplemental Table 5.

H) ATAC-seq and ChIP-seq tracks at the *IFNG*, *IL2RA,* and *TOX* loci.

A-C) Pooled data from $n = 3$ donors.

F and H) One representative donor of $n = 3$ donors.

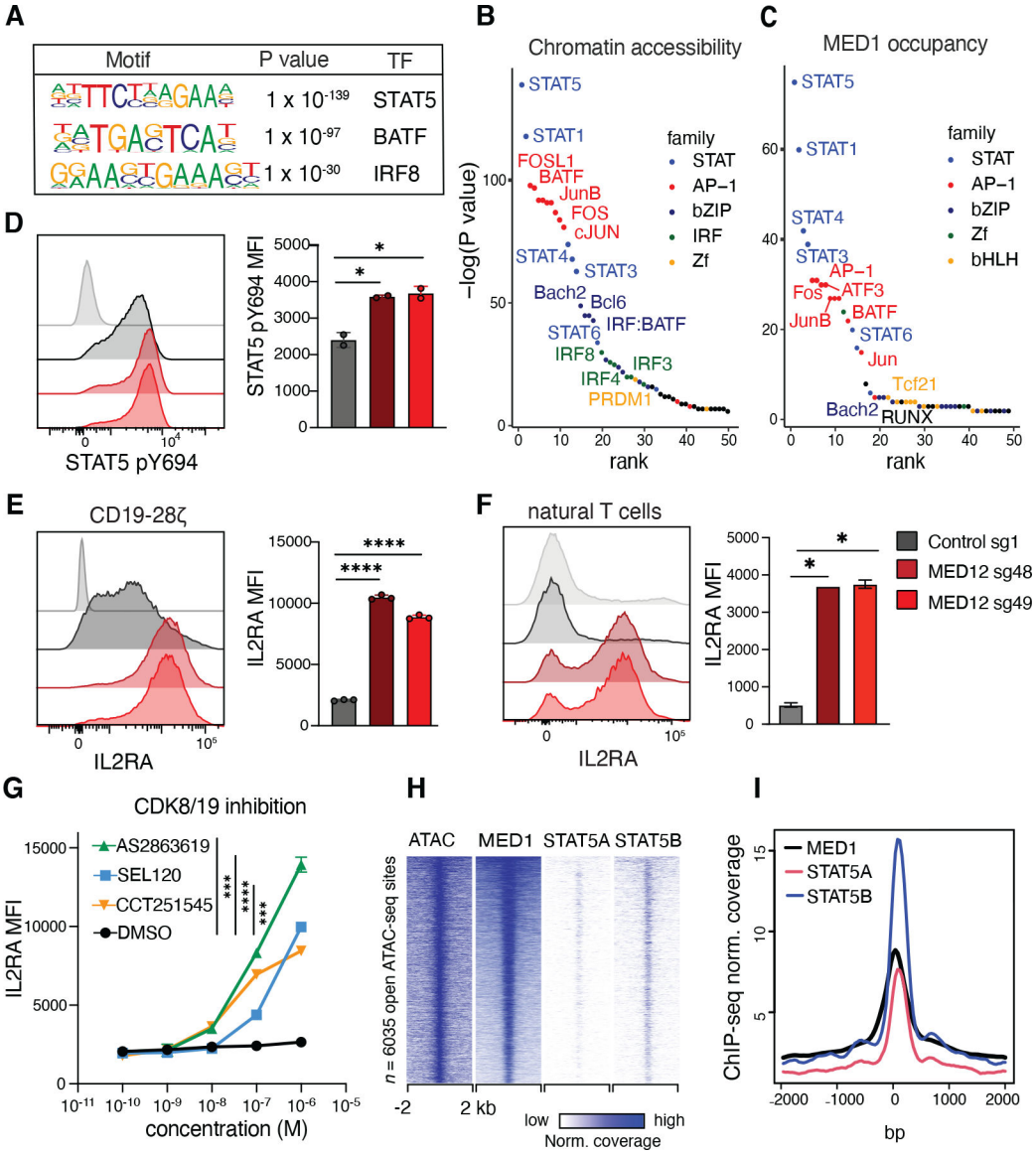

Fig. 7. Loss of *MED12* increases STAT5 activity in CD19–28ζ CAR-T cells

A and B) Transcription factor binding motif enrichment at sites with increased chromatin accessibility by ATAC-seq in resting *MED12* deficient CD19–28ζ CAR-T cells 15 days post T cell activation. $n = 6035$ sites with Log2FC > 1 and adj. $P < 0.05$.

C) Transcription factor binding motif enrichment at sites with increased MED1 occupancy by ChIP-seq in resting *MED12* deficient CD19–28ζ CAR-T cells. $n = 842$ sites with adjusted $P < 0.05$.

D) Flow cytometry analysis of STAT5 phosphorylation in control and *MED12* deficient CD19–28ζ CAR-T cells 15 days post T cell activation. Cells were cultured *in vitro* with continuous IL-2. The cells shown in light grey were rested without IL-2 for 24 hours prior to staining.

E and F) Flow cytometry analysis of IL2RA expression in control and *MED12* deficient F) CD19–28ζ CAR-T cells or G) non-transduced T cells 15 days post activation. Control staining with isotype antibody is shown in light grey.

G) Flow cytometry analysis of IL2RA expression in non-transduced T cells cultured with dual inhibitors of CDK8 and CDK19 for 15 days. Inhibitors were supplemented to the culture medium every 48 hours.

H) Heatmaps of genomic loci with significantly increased chromatin accessibility by ATAC-seq in *MED12* deficient CD19–28ζ CAR-T cells. Genomic loci are overlaid with ATAC-seq and MED1 ChIP-seq signal from resting CD19–28ζ CAR-T cells 15 days post T cell activation. STAT5A and STAT5B ChIP-seq data was obtained from human $CD4^+$ T cells stimulated with IL-2 (GEO accessions GSM671400, GSM671402).

I) Mean ChIP-seq signal intensities at $n = 6035$ sites corresponding to panel H.

A-C) Pooled data from $n = 3$ donors. Homer motif enrichment was performed with a set of all A and B) ATAC-seq or C) MED1 ChIP-seq peaks detected in CAR-T cells as the background.

D-G) Data are mean ± s.d. from $n = 2–3$ wells. Representative results from two independent experiments. Two-tailed unpaired Student's *t*-test. $*P < 0.05$, $**P < 0.01$, $***P < 0.001$, $****P < 0.0001$

H-I) One representative donor of $n = 3$ donors.